

On the characteristics of earthquake stress release variations in Japan

Adrien Oth

European Center for Geodynamics and Seismology (ECGS)
19 rue Josy Welter, L-7256 Walferdange, Grand Duchy of Luxembourg.

Email: adrien.oth@ecgs.lu

Tel: +352 331487-35

Fax: +352 331487-88

Earth Planet. Sci. Lett., 377-378, 132-141

doi : 10.1016/j.epsl.2013.06.037

Highlights

- Earthquake stress release in Japan shows systematic lateral variations.
- Crustal earthquake stress drop variations are largely thermally driven.
- High subcrustal earthquake stress drops in regions of strong subduction-interface coupling.
- Stress drop scale-dependence is highly variable and locally non-self-similar.
- Stress release variability on local scale is only $\frac{1}{2}$ - $\frac{1}{3}$ of full region variability.

Abstract

The amount of stress released during earthquakes is a fundamental characteristic of the earthquake rupture process. As such, it represents a key parameter for improving our understanding of earthquake source physics and for reliable ground motion prediction. Large earthquake populations usually show variations in stress release as large as three orders of magnitude, but the underlying mechanisms have remained largely elusive, and particularly the dependence of stress release on earthquake size is still a matter of debate. Here I use a unique dataset from Japan encompassing earthquakes of a wide magnitude range and spatial coverage to show that stress release variations of crustal earthquakes are strongly correlated with heat flow variations, indicating that they are thermally controlled. In contrast, subcrustal events depict highest stress release in regions of strong subduction-interface coupling and overall less pronounced variability as compared with crustal earthquakes. Stress release is overall only weakly dependent on earthquake size, but at local scales (i.e., within individual earthquake sequences) the dependence can be very strong and apparently varies with stress regime. Accounting for these systematic variations reduces the stress release variability on local scale by a factor of two to three as compared with the full earthquake population, a finding that is of key significance in the endeavor to reduce the uncertainties in future ground motion predictions.

Keywords: Stress drop; Japan; earthquake source scaling; earthquake physics; earthquake ground motions

1. Introduction

During the past decades, compelling evidence has been provided that the rupture dynamics of the seismic source process must span an extraordinarily wide range between the end members of slow earthquakes (Beroza and Ide, 2011) and super-shear ruptures (Das, 2007). One of the most important characteristics of the earthquake source process is the amount of stress released on the fault, often referred to as stress drop.

By itself, stress drop has no direct link to the energy radiated as seismic waves during a seismic event. For example, creep events do not radiate any seismic energy, yet the associated stress drop can be measured geodetically. For small to moderate-size earthquakes, stress drop is however often linked to the seismic energy radiation via specific models that involve dynamical representations of the seismic source (e.g., Brune, 1970, 1971; Madariaga, 1976). While as a matter of principle, radiated energy can be determined without any model assumptions (usually via integration in the frequency domain), the adoption of a specific source model is nevertheless often required in practice in order to overcome bandwidth limitations of the seismic data (e.g., Ide and Beroza, 2001). In the context of such a given source model, seismically determined stress drop can thus be considered to be a parameter providing hints on the physics of the rupture processes (Kanamori and Heaton, 2000; Abercrombie and Rice, 2005) and is of key importance for reliable ground motion prediction (Cotton et al., 2013), yet the relation between the stress drop and radiated energy is strongly model-dependent.

Stress drop estimates have proven to be highly variable, covering about three orders of magnitude (mostly the range 0.1 – 50 MPa, Abercrombie and Rice, 2005; Shearer et al., 2006; Allmann and Shearer, 2009; Oth et al., 2010, the absolute values

however depending on the selected source model), and the question as to what causes this variability could thus far only be speculated upon. In a detailed study involving more than 60,000 small earthquakes (local magnitude $M_L \leq 3.1$) in southern California, Shearer et al. (2006) observed spatially coherent stress drop variations, but no simple link with potential tectonic causes was discernible. On global scale and the other end of the magnitude scale, Allmann and Shearer (2009) investigated the stress drops of about 2000 moderate to large earthquakes (body wave magnitude $m_B \geq 5.5$) and found a high degree of variability as well as some degree of dependence on focal mechanism and tectonic province.

Besides this high degree of variability, large earthquake populations are usually characterized by weak (if any) stress drop dependencies on earthquake size (i.e., seismic moment, e.g., Shearer et al., 2006; Allmann and Shearer, 2009; Oth et al., 2010). Contrasting these findings, a range of studies based on individual earthquake sequence data (thus dealing with events taking place on a significantly more localized spatial scale) provided evidence for a sometimes-considerable stress drop and/or scaled energy (ratio of radiated energy E_R to seismic moment M_0) increase with increasing earthquake size (Mayeda et al., 2005). However, conflicting results were obtained in various cases (e.g., Mayeda and Malagnini, 2010; Baltay et al., 2010) and methodological aspects often hamper the direct comparison of contradicting findings.

In order to obtain new insights that might help to clarify these issues, I study the stress drop variations of 3964 earthquakes that occurred throughout Japan from May 1996 to October 2011, ranging in moment magnitude (M_W) from 2.7 to 7.9 and including events from 12 particular major sequences (Fig. 1, Tables S1 and S2 in the supplementary material). This uniformly processed dataset allows for a robust quantification not only of potential systematic lateral stress release variations on the

scale of the Japanese archipelago, but also of the stress drop scaling with earthquake size on the local scale of individual earthquake sequences, and its variability throughout the country. Combined with the availability of reliable information on focal mechanisms, b values, heat flow and geodetic strain rates in Japan, this dataset provides highly favorable conditions in the quest for the causes underlying earthquake stress release variations.

2. Data and Methods

Stress drop estimates were calculated based on the S-wave source spectra derived from ground motions recorded at the KiK-net and K-NET accelerometric networks (Okada et al., 2004). For simplicity and consistency with Oth et al. (2011) we refer to earthquakes shallower than 30 km as crustal, although it should be recognized that a small number of these might actually be in the upper mantle. Events with depths larger than 30 km are termed as subcrustal and generally subduction-related (see also Fig. 2 of Oth et al., 2011).

2.1 Spectral Inversion

For separation of the observed S-wave Fourier amplitude spectra into their (acceleration) source spectra, attenuation and site response contributions, I use the processing procedures and one-step non-parametric generalized inversion technique (GIT) detailed in Oth et al. (2011). This approach is a variant of the spectral inversion scheme first proposed by Castro et al. (1990) and is particularly well suited for the case of large datasets where each station recorded several (or a large number of) events and each event has been recorded by several stations. At a given frequency, the ground motion spectra in log domain are considered as a linear combination of a source, a site and an attenuation term, the latter depending on hypocentral distance. In

particular, the functional form of the attenuation operator does not need to be pre-defined, a fact that allows for attenuation correction without specific model assumptions on Q or geometrical spreading. The only constraints required are that (1) the attenuation operator is set to a given value (usually unity) at a given reference distance R_0 (for which I use $R_0=5$ km, as this is the minimum distance well covered by the data in Japan) and (2) attenuation varies smoothly with distance (see for instance Castro et al., 1990, for the implementation of these constraints).

Thus, attenuation is taken into account via a 1D, non-parametric model (ranging from the reference distance of 5 km up to a maximum hypocentral distance of 250 km). In order to compensate at least to some degree for the fact that these attenuation curves are merely 1D models and to account for potential regional attenuation variations (since in particular crustal attenuation in Japan as a whole may not be well described by a single 1D model), different crustal attenuation models were derived for Kyushu, southern Honshu/Shikoku as well as the fore- and backarc regions of northern/central Honshu (Oth et al., 2011). Furthermore, separate attenuation functions were determined for crustal and subcrustal events, since the propagation paths for seismic waves traveling to the surface are very different for shallow crustal and upper-mantle earthquakes. The attenuation operator for subcrustal events can however only be used to correct attenuation down to a subcrustal reference distance of 30 km, and for the attenuation correction of the remaining travel path in the crust down to the general reference distance of 5 km used in this article, the respective crustal attenuation functions are applied (Oth et al., 2011).

The attenuation-corrected spectra are then separated into their source and site contributions. For this purpose, a reference condition needs to be set either for the source or for the site term, since otherwise there is an unconstrained degree of

freedom in the inversion (as stated by Castro et al., 1990, an arbitrary function of frequency could be added to either term and subtracted from the other, with the same fit to the data). For the borehole dataset (see below), I use the reference condition that the average of the site response of all stations equals unity, independent of frequency, while for the surface dataset, a well-suited rock site is used as reference station (Oth et al., 2011).

The least squares inversions are performed individually for a discrete set of 40 frequency points equidistant on log scale in the range 0.5 – 25 Hz. In summary, the spectral inversion approach thus leads to frequency-dependent, non-parametric solutions for source spectra (attenuation-corrected to the reference distance of 5 km), attenuation and site terms, with appropriate constraints for attenuation and site response. For additional details on the methodological aspects as well as a full discussion of source spectral shapes, attenuation characteristics and site response functions, I refer the reader to Oth et al. (2011) and the references therein.

The dataset used is a significantly extended version from previous work (Oth et al., 2010, 2011). Separate inversions were run for surface and borehole recordings. In total, 113,372 records obtained at 1637 surface stations (KiK-net and K-NET) from 4188 events and 53,394 records at 674 borehole stations (KiK-net only) from 3579 events were processed. Only weak and not too strong ground motions (peak ground accelerations lower than 0.2g) were considered in order to minimize potentially nonlinear site response and exclude near-field recordings of large events. As mentioned earlier, the regional non-parametric attenuation functions are as such only 1D models (Oth et al., 2011), and one might raise the concern that near-source 2D/3D attenuation variations could bias the observed lateral stress drop variations discussed below. However, as I discuss in section 1 of the supplementary material, such 2D/3D

attenuation variations can be shown to represent an unlikely, or at least not an obvious source of bias.

2.2 Seismic moment (M_0), corner frequency (f_c) and stress drop ($\Delta\sigma$)

If available, the source spectra derived from borehole records were used since these are less prone for residual site effect contamination and are much less affected by the problem of high-frequency amplitude diminution (κ or f_{\max} effect, Hanks, 1982; Anderson and Hough, 1984; see Oth et al., 2011, for a detailed discussion of how this effect was taken into consideration). This was the case for 85% of all events. In the case of source spectra determined using the surface recordings, these were empirically corrected to borehole reference level using a well-constrained empirical correction function (Oth et al., 2011).

Source spectral fits with the ω^2 -model (Brune, 1970, 1971) were carried out to determine corner frequency f_c and seismic moment M_0 (respectively moment magnitude M_w), using nonlinear least squares (Oth et al., 2010):

$$S(f) = (2\pi f)^2 \frac{R^{\theta\phi} V F}{4\pi\rho v_s^3 R_0} \dot{M}(f) \quad \text{with} \quad \dot{M}(f) = \frac{M_0}{1 + (f/f_c)^2}, \quad (1)$$

where $S(f)$ represents the acceleration source spectrum at the reference distance $R_0=5$ km. $\dot{M}(f)$ denotes the moment-rate spectrum, $R^{\theta\phi}$ the average radiation pattern of S-waves set to 0.55 (Boore and Boatwright, 1984), $V = 1/\sqrt{2}$ accounts for the separation of S-wave energy onto two horizontal components, $F = 2$ is the free surface factor and ρ and v_s are material parameters, i.e., density and shear-wave velocity.

The last two parameters were set to $\rho=2.9$ g/cm³, $v_s=3.0$ km/s for crustal and $\rho=2.9$ g/cm³, $v_s=3.3$ km/s for subcrustal events, respectively. For large events with Japan Meteorological Agency (JMA) magnitude $M_{\text{JMA}} \geq 5$, f_c is likely to be smaller than the

lowest frequency in the analysis and M_0 was constrained to the value given in the regional moment tensor catalog of the National Institute for Earth Science and Disaster Prevention (NIED) (*The NIED CMT solutions*, <http://www.fnet.bosai.go.jp>). In other words, this means that for the larger events in the dataset, I rely on the assumption that the ω^2 -model holds, and determine the corner frequency from the high-frequency plateau level (which can be done if the seismic moment is constrained from another source). Note that the density and velocity values given above were chosen such that the seismic moments of events with $M_{JMA} < 5$ as determined from the spectral fitting procedure are fully compatible with the NIED CMT solutions, and therefore also with the moments used as constraints for the large events. This is important in order to avoid bias in the scaling trends due to incompatible moments between small and large earthquakes (more details are provided in section 3.3. and the supplementary material, section 2).

3964 of the 4188 events had well-constrained source spectra, characterized by robust nonlinear least squares fits using the ω^2 -model (we removed unreliable source spectra with root-mean-square deviation from the ω^2 -fit larger than twice the average rms or very large corner frequency error estimates resulting from the spectral fit of more than 50% of the estimated value).

Stress drop $\Delta\sigma$ was computed following Hanks and Thatcher (1972):

$$\Delta\sigma = 8.5 M_0 \left(\frac{f_c}{v_s} \right)^3, \quad (2)$$

where $v_s=3.0$ km/s for crustal (depth ≤ 30 km) and $v_s=3.3$ km/s for subcrustal events (depth > 30 km), respectively, and I will discuss potential biasing effects resulting from the usage of these fixed values further below. It should be noted that equation (2) assumes validity of the Brune (1970, 1971) model, and stress drop estimates differ

by a factor of 5.5 between the commonly used models of Brune (1970, 1971) and Madariaga (1976), the latter leading to higher estimates. Radiated energy E_R was determined by integration over the S-wave source spectra, where extrapolation beyond the bandwidth of analysis may be required and was taken into consideration (Ide and Beroza, 2001; Oth et al., 2010).

It has been shown that scaled energy is strongly correlated with stress drop (Oth et al., 2010, Fig. S1 in the supplementary material), a fact that is also theoretically expected as far as the source spectra can be described by the ω^2 -model (Brune, 1970, 1971; see also Singh and Ordaz, 1994) and in particular if extrapolation beyond the bandwidth limits is carried out under the assumption that the ω^2 -model holds. Therefore, the discussion in the following is solely based on stress drop variations, and the conclusions apply likewise to scaled energy. Finally, similar to spectral ratio respectively empirical Green's functions (EGF) approaches, the most robust component of the results obtained with the methods described above lies in relative stress drop variations between near-by events located at similar depths.

2.3 Stress drop scale-dependence

The stress drop scale-dependence is quantified using the ϵ parameter (Kanamori and Rivera, 2004), such that $M_0 \propto f_C^{-(3+\epsilon)}$. For each earthquake sequence respectively data subset, ϵ is calculated based on linear regression of $\log f_C$ vs. $\log M_0$ data, and an estimate of the standard deviation is computed from 100 bootstrap samples. ϵ is a measure of how strongly stress drop changes with varying seismic moment. Following equation (2), if $\Delta\sigma$ is constant irrespectively of seismic moment, $M_0 \propto f_C^{-3}$, and thus $\epsilon=0$ represents self-similar stress drop scaling. In contrast, if $\Delta\sigma$ increases

with increasing seismic moment, f_C decays slower with increasing M_0 , leading to $\epsilon > 0$.

In the opposite case of decreasing $\Delta\sigma$ with increasing M_0 , $\epsilon < 0$.

2.4 Faulting style classification

Faulting style was classified into thrust, strike-slip and normal faulting using the plunges of P- and T-axes (Appendix D in Boore and Atkinson, 2007). For visual representation however, the rake-based classification approach introduced by Shearer et al. (2006) was used, which provides values on a continuous scale ranging from -1 (normal) via 0 (strike-slip) to +1 (thrust). Both approaches lead to nearly the same classification when the range of normal faulting events in the rake-based approach is fixed to [-1 -0.25], strike-slip to [-0.25 0.25] and thrust to [0.25 1] (for crustal events, 93% of normal, 98% of thrust and 94% of strike-slip events are classified identically with both approaches). Faulting style at a given location in Japan is generally not strongly variable (Fig. S2b in the supplementary material), and hence the lateral stress drop variations discussed below do not change if separate variation maps are generated for each type of faulting alone.

2.5 Lateral variation maps

Lateral variation maps for stress drop, faulting style and heat flow were calculated on a $0.1^\circ \times 0.1^\circ$ grid applying a spatially weighted averaging function (Gaussian smoother, Fig. S3 in the supplementary material) within a radius of 50 km around each grid point, weighting the influence of the individual earthquakes respectively measurement locations in relation to their distance to the grid point. This procedure was used separately for the crustal and subcrustal event sets, and apart from this separation, focal depth is not specifically accounted for in the lateral variation maps (the depth-dependence of stress drop is separately discussed in section 3.3). Weighted average and standard deviation were only retained if at least 5 data points

were available in the spatial window. The residual strain rate data (see section 3, Mazzotti et al., 2001) were interpolated from their original $1/3^\circ \times 1/3^\circ$ grid to the same 0.1° by 0.1° grid as for the stress drop lateral variations, and the b value data (see section 3, Toda and Enescu, 2011) were already provided on a 0.1° by 0.1° grid.

2.6 Extraction of individual earthquake sequences for separate analysis

Individual earthquake sequences have been extracted from the total event set by considering earthquakes in a time window of six months within a lateral range of one estimated fault length (Wells and Coppersmith, 1994) from the mainshock, and one estimated fault width in depth. While this represents a very rough first order selection criterion, it worked generally well in selecting subsets that outline the lateral extent of mainshock fault planes as compared to literature estimates. The scaling results obtained from these data subsets did not substantially change when using for instance shorter time windows (such as three months) or a slightly larger spatial window. For the Tohoku-Oki earthquake, the geometry of the mainshock fault plane was taken from the literature (Suzuki et al., 2011).

3. Lateral stress drop variations and focal-depth dependence

3.1 Crustal earthquakes (depth range ≤ 30 km)

Crustal earthquake stress drops depict clear systematic lateral variations with about two orders of magnitude difference between lowest and highest stress drop regions (Fig. 2a), which is by far larger than the variability in each local sample (standard deviation on the order of 0.3 with a maximum of 0.6 log-units, Fig. S2a in the supplementary material). A significantly increased stress drop level is found in Kyushu (~ 3 -20 MPa, see Fig. 1 for region denomination) as compared with Honshu (~ 0.1 -3MPa), most notably for the 2005 Fukuoka sequence (Fig. 3).

Earthquake faulting mechanisms vary systematically as well (Fig. 2b), and the spatial stress drop pattern could therefore be the consequence of focal-mechanism dependence. Indeed, a slight stress drop trend with varying focal mechanism can be seen (Fig. 4), most notably a very large stress drop variability for strike-slip earthquakes (faulting style parameter zero in Fig. 4) and a tendency for slightly higher stress drops in strike-slip and normal faulting events as compared to thrust events. This finding is contrary to the expectations arising from Andersonian faulting theory, as far as stress drop is assumed to be proportional to differential stress, but has also been occasionally found in previous studies (Shearer et al., 2006; Allmann and Shearer, 2009).

However, a look at Fig. 2a also shows that strike-slip earthquakes depict distinctly different stress drop samples in Honshu and Kyushu, and it is this strong lateral variation that explains the very large overall scatter observed for strike-slip events (Fig. 3). Normal faulting earthquakes in Honshu almost all belong to the unusual shallow normal faulting activity around Iwaki following the 2011 Tohoku-Oki earthquake (Fig. 2b, Imanishi et al., 2012; Yoshida et al., 2012). While their stress drops seem to be slightly higher than the ones of thrust and strike-slip events in Honshu, they are much lower than those of normal faulting events in Kyushu (Figs. 2a, 3). A two-sample KS-test rejects the null hypothesis that the Honshu/Kyushu strike-slip respectively normal faulting stress drop samples are drawn from the same distribution at a significance level of 1%. In contrast, the few thrust events offshore western Kyushu show stress drops similar to those obtained in central Honshu (non-volcanic region). The sum of these observations suggests that the apparent focal-mechanism dependence seen in Figure 4 is instead related to lateral variation and

some other mechanism besides the stress regime must come into play in order to explain the observed stress drop variations.

Low stress drop earthquakes in Honshu occur systematically in proximity of quaternary volcanoes (Fig. 2a, Nakano et al., 2001). Volcanic activity involves increased temperatures in the crust as well as the likely presence of fluids (Hasegawa et al., 2009), and thus potentially increased pore fluid pressure. The latter is known as a factor lowering effective normal stress and is therefore recognized as a potential cause for low stress drop earthquakes (Goertz-Allmann and Wiemer, 2013). Since it is very likely that attenuation is also strong in volcanic regions, lateral attenuation variations could be a potential source of bias affecting the source spectra, and thus the stress drop estimates. However, the tests described in the supplementary material (section 1) do not show any evident hints for the existence of such a bias.

In relation to the apparent link between low stress drop earthquakes and the presence of quaternary volcanoes, crustal temperature variations (which are a controlling factor for frictional strength variations) are an obvious candidate as a driving mechanism for the observed stress release variations. Heat flow serves as a proxy for the thermal state of the crust and has been estimated throughout Japan from geothermal gradient data (Fig. 2c, Tanaka et al., 2004). It was shown to be the dominant factor controlling the thickness of the seismogenic layer (Tanaka, 2004), and the excellent spatial correlation of low stress drop with high heat flow areas in Honshu (Fig. 5) provides compelling evidence that the lateral variations of crustal earthquake stress drops are thermally controlled as well. This inverse correlation of stress drop with heat flow variations, even though somewhat more ambiguous, seems to apply to Kyushu as well, but at higher average stress drop level. Stress drops of individual earthquake sequences are consistent in the framework of the above

observations and show significantly lower variability, of the order of one to one-and-a-half orders of magnitude (Fig. 3).

Crustal deformation rate is nowadays commonly considered in seismic hazard models since it can be viewed as a proxy for earthquake potential, and may also be a contributing factor to the observed stress drop variations. In central Japan, the Niigata-Kobe tectonic zone (NKTZ) is such a zone of high strain rate (Sagiya et al., 2000), with large shear-strain rates in its southern and central parts (Fig. 2d, geodetic estimates corrected for subduction-related interseismic deformation, Mazzotti et al., 2001). Stress drops are indeed higher (1-3 MPa) in the south, where heat flow is low, yet drop to low values (~0.1-0.5 MPa) in the volcanic area in the center of the NKTZ, where both strain rate and heat flow are elevated. While stress drop variations show a distinct spatial correlation with heat flow variations (compare Figs. 2a, c, Fig. 5), this is much less the case with the geodetic strain rate estimates (compare Figs. 2a, d).

Toda and Enescu (2011) calculated lateral b -value variations throughout Japan using the JMA earthquake catalog from January 1998 to December 2008 and a maximum likelihood procedure, considering earthquakes of $M_{\text{JMA}} \geq 2.2$ at crustal depths (depth ≤ 30 km, Fig. 2e). It has been previously hypothesized that b values are related to faulting style, with lowest values for thrust and highest for normal faulting, thus directly reflecting an inverse correlation with differential stress (Schorlemmer et al., 2005).

Similar to what has been observed in southern California (Shearer et al., 2006), the b -value variations in Japan show neither an evident link with faulting style variations nor with stress drop variations. For instance, regions of strike-slip faulting show a large variety of b values, with low values in the area of the 2005 Fukuoka sequence in northern Kyushu and higher values in southern Honshu. If stress drop is

assumed proportional and b values inversely proportional to differential stress, this result by itself could simply be interpreted to be indicative of the possible variation range of differential stress within a strike-slip faulting regime. However, the b values in the area of the 2005 Fukuoka sequence show similar levels as they do in areas of thrust faulting in northern Honshu, where stress drops are low, and in the area of normal faulting in central Kyushu, the b values are not significantly larger than elsewhere. In addition, b values are also very low in the region of the shallow normal faulting activity in northeastern Honshu, but this observation needs to be interpreted with caution, since the pronounced normal faulting activity was only activated in the aftermath of the 2011 Tohoku-Oki event (Imanishi et al., 2012; Kato et al., 2013), which significantly changed the stress field situation in this region, yet the b values shown in Fig. 2e were derived from an earlier catalog.

Finally, there is no such systematic decrease in b values in Kyushu as the observed systematic increase in stress drop level would suggest via the assumed link through differential stress. These observations therefore either suggest that stress drop cannot be considered to be related to differential stress in such a simple way, or that besides the hypothesized inverse correlation between b values and differential stress (Schorlemmer et al., 2005), other factors must influence the b value variations as well.

3.2 Subcrustal earthquakes (depth range ≥ 30 km)

Subcrustal earthquakes show stress drops higher by one order of magnitude (median ~ 10 MPa) than their crustal counterparts (median ~ 1 -2 MPa). It should however be noted at this point that, depending on the assumed combination of density and velocity estimates in the spectral fitting and stress drop calculation (equations 1 and 2, see also section 3.3), the very large difference between the absolute stress drop

levels of subcrustal and crustal events could diminish to some extent. Relative variations among subcrustal events are unaffected by this issue.

Subcrustal events also depict overall lower stress drop variability (one order of magnitude lower, Fig. 6). Apart from the Kushiro-Oki sequence, a two-sample KS-test between different samples at 10% confidence level cannot reject the null hypothesis of these emanating from the same distribution. They furthermore show no dependence on faulting mechanism (Fig. 4), providing hints for similar average stress release in subduction-interface and in-slab events. Nonetheless, some relevant lateral features are also apparent in the subcrustal case (Fig. 7). The largest stress drops are found in southeastern and offshore Hokkaido as well as offshore Miyagi, in the southern and central parts of the 2011 Tohoku-Oki fault plane. These regions of high stress release are consistent with zones of strong subduction-interface coupling (Hasegawa et al., 2009; Hashimoto et al., 2009) and with the areas of high seismic energy release during the Tohoku-Oki event (Kurahashi and Irikura, 2013; Ide et al., 2011).

3.3 Focal-depth-dependence

Similar to what was found in some previous studies (Shearer et al., 2006; Allmann and Shearer, 2007), stress drop also shows a gentle increase with focal depth, from an average of ~ 1 MPa in the upper 10 km to ~ 4 MPa at 30 km and up to ~ 15 MPa at 100 km depth (Fig. 8). This is not necessarily unexpected, at least to the extent as proportionality of stress drop with differential stress is assumed. Yet in light of the large lateral stress drop variations for crustal earthquakes of about two orders of magnitude, the observed increase from 1 to about 4 MPa over the crustal depth range is very subtle.

It has also been found previously that accounting for the depth-dependence of shear-wave velocity v_S (and with v_S , implicitly also the depth-dependence of rupture velocity) may explain the apparent depth-dependence (Allmann and Shearer, 2007). In order to verify in how far the observed increase with depth could thus simply be due to neglecting the depth-dependence of the material parameters ρ and v_S , I investigated the outcome of the spectral fitting procedure under the assumption of depth-variable material parameters. I adopted the 1D JMA2001 velocity model (Ueno et al., 2002), and the depth-dependence of density was estimated through empirical relationships between ρ and P-wave velocity v_P , using Gardner's rule (Gardner et al., 1974) for $v_P < 6$ km/s and the Nafe-Drake curve (Brocher, 2005) for $v_P \geq 6$ km/s.

Figure 9 shows the depth-dependent effect on v_S^3 , M_0 and $\Delta\sigma$ (ratios relative to the values obtained with constant ρ and v_S). In the depth ranges where most of the earthquakes are located, the effect on stress drop is extremely small, since with increasing ρ and v_S , M_0 derived from equation (1) increases as well, approximately balancing when calculating stress drop. Thus, accounting for the depth-dependence of ρ and v_S in the spectral fits neither significantly changes the absolute level of stress drop estimates nor their depth-dependence. However, it should be noted that the seismic moments are then somewhat higher than those of the NIED CMT solutions, leading to M_W values larger by on average 0.12 units for crustal and 0.35 units for subcrustal events, and this inconsistency with the NIED CMT solutions would lead to a potential bias in the determination of the stress drop scale-dependence (see also supplementary material section 2).

The fact that the adjustments needed in order to be consistent with the NIED solutions are larger for subcrustal events could hint towards an overall slightly too strong attenuation correction for this event type. As mentioned above in section 3.2,

this could mean that the general difference in absolute stress drop level between crustal and subcrustal events is somewhat overestimated. However, it should be noted in this context that for a given seismic moment, corner frequencies of subcrustal events are on average higher by a factor of about two than those of their crustal counterparts.

Nonetheless, I conclude from this analysis that the increase of stress drop with depth observed in Japan is not that easily attributable to the assumption of constant rupture velocity in stress drop calculation, at least not when considering the 1D JMA2001 velocity model.

4. Stress drop scaling with earthquake size

Taken altogether stress drop only shows a weak dependence on earthquake size (ϵ only slightly positive), both for crustal and subcrustal events, but scale-dependence does depict prominent variations between individual earthquake sequences and across different stress regimes (Fig. 10). This finding resolves the apparent contradiction between strong non-self-similarity obtained in some studies based on individual sequence data (Mayeda et al., 2005) and close to self-similar scaling derived from large earthquake populations (e.g., Allmann and Shearer, 2009; Oth et al., 2010), showing that strong yet localized scale-dependencies tend to be averaged out in large earthquake populations. While crustal strike-slip earthquakes show highest variability in stress drop level (Fig. 3), their scale-dependence shows the smallest variations, close to self-similarity (ϵ close to zero). In contrast, crustal thrust events in Honshu show a strong stress drop increase with seismic moment, with sequence ϵ values reaching up to one. As opposed to Honshu, ϵ is always negative in Kyushu (trend for decreasing stress drop with increasing seismic moment), while the normal faulting

events in northeastern Honshu depict large positive ϵ . Compared to crustal earthquakes, subcrustal events show relatively little ϵ -variations, with slightly higher ϵ for normal faulting relative to strike-slip and thrust events.

The 2011 Tohoku-Oki M_w 9.0 mainshock was not included in the spectral inversion since it has been shown that this event entailed a clear separation of areas radiating dominantly low-frequency (shallow part of the fault plane close to the trench) and high-frequency (deep part of the rupture) energy (e.g., Ide et al., 2011). From this perspective, this extraordinary megathrust earthquake is thus too complex to be treated in the simple framework of the ω^2 -model. Instead, it is nevertheless interesting to verify whether the areas of the rupture plane that produced strong high-frequency energy release show stress drops consistent with what would be expected from the stress drop scaling relation as discussed in this article. Such areas of high-frequency energy release have also been termed as *strong motion generation areas* (SMGAs) in the literature (e.g. Miyake et al., 2003; Kurahashi and Irikura, 2013).

The sequence as treated in the spectral inversion thus only included the M_w 7.2 foreshock as largest event. Figure 11 shows the scaling of the sequence as it originated from the spectral inversion, which is in excellent agreement with the expectation for subcrustal thrust events (Fig. 10), both in stress drop level and scaling behavior. Note that the ϵ estimate shown in Fig. 11 has been derived without the SMGA stress drop estimates of the 2011 Tohoku-Oki earthquake. The latter were determined using empirical Green's functions modeling (Kurahashi and Irikura, 2013) and range from 16 to 26 MPa, which is at the upper bound of the range expected for subcrustal thrust events of these magnitudes when extrapolating along the ϵ dependence. This result indicates that these SMGAs indeed dominantly radiate high-frequency energy and thus can be seen as a representation of high-frequency

subevents of the 2011 Tohoku-Oki earthquake. Furthermore, they were consistently located in areas of overall slightly increased stress drops as compared with the surroundings of the 2011 Tohoku-Oki fault plane (Fig. 7).

5. Discussion and conclusions

The potential influences of a range of factors (i.e., stress regime, focal depth, crustal strain rate, heat flow and frequency-magnitude distribution respectively b value) on lateral stress release variability in Japan have been discussed above, and the outcome of this study provides compelling evidence that crustal earthquake stress drops in Japan are primarily thermally controlled. Furthermore, due to the evident link between areas of high heat flow and volcanic centers, increased pore fluid pressure in relation to the volcanic activity most likely also plays a significant role. The consistently non-self-similar scaling property of increasing stress drop with increasing earthquake size in crustal earthquake sequences in northern Honshu provides further indications in that direction. Indeed, a potential explanation often invoked for increased stress drop and seismic energy release from larger earthquakes is given by dynamic frictional weakening and fault lubrication with increasing fault slip (Malagnini et al., 2010), in agreement with laboratory observations under seismic slip rates (Di Toro et al., 2011). The strongly positive ϵ values in northern Honshu are consistent with this argument, and an increased level of pore fluid pressure in the volcanic areas could further facilitate such a weakening mechanism.

As for the average stress drop level that is one to two orders of magnitude higher as compared with Honshu, Kyushu also clearly sets apart in terms of scaling behavior, showing a general tendency for decreasing stress drop with increasing seismic moment. While crustal thrust and apparently also normal faulting earthquakes

(even though apart from the shallow normal faulting activity in northeastern Honshu triggered by the Tohoku-Oki earthquake, no individual earthquake sequences with normal faulting mechanism are available) show large ranges of variation in their scaling characteristics, crustal strike-slip earthquakes seem to be much less sensitive to the factors causing these variations and overall tend to show close to self-similar scaling within the uncertainty bounds, no matter their location. It should be noted however that the scaling trends in Kyushu (Fig. 10) are not very well constrained for normal faulting (very limited M_w range 3.2-4.4, Table S1) and thrust (reasonable M_w range 3.3-6.0, but only 18 events) earthquakes.

Nonetheless, the combination of high crustal stress drops and negative ϵ in Kyushu is remarkably different from Honshu and cannot be explained only with the above hypotheses, but Kyushu also shows tectonic peculiarities that cannot be explained solely on the basis of plate interaction or structural variations. In contrast to northern Honshu and central-southwest Japan, it depicts a more complex stress field with tensional features and a horizontal stress gradient (Seno, 1999). The higher average stress drop level and diverging scaling trend might thus be the consequence of these peculiarities. These complications notwithstanding, also the lateral stress drop variations in Kyushu seem to correlate with heat flow variations, even though admittedly to a less evident extent than in Honshu and at higher average stress drop level.

Subcrustal earthquakes show high stress drops in region of estimated strong subduction-interface coupling (Hasegawa et al., 2009; Hashimoto et al., 2009), and in the context of the Tohoku-Oki earthquake, elevated stress drops are found in the down-dip areas where also high seismic energy release took place during this megathrust rupture (Kurahashi and Irikura, 2013; Ide et al., 2011). The slight increase

in scale-dependence for subcrustal normal faulting events may be related to the different causative mechanisms for in-slab (dominantly normal faulting) and subduction-interface (dominantly thrust) events (Choy and Kirby, 2004), even though no difference between these can be seen in the average stress drop level. In combination with the scaling information, stress drops determined in this study for small to moderate earthquakes taking place in highly coupled asperity regions of the subduction interface may provide useful constraints for ground motion simulations of major earthquakes in these areas in the future.

The findings of this study represent a key element for reducing uncertainties in ground motion predictions in Japan, in particular for major inland crustal earthquakes. Earthquake stress release shows strong systematic lateral variations with local variability of around one to one-and-a-half orders of magnitude, which is significantly smaller than the overall variability of three orders of magnitude. For this reason, the use of regionally appropriate stress parameters for ground motion prediction is imperative. Stress release dependence on the thermal state of the crust should be considered in shaking hazard assessment procedures, and for ground motion simulations based on up-scaling of small event recordings, the usage of appropriate scaling parameters that may considerably deviate from the often-used self-similarity assumption is essential.

Acknowledgements

I thank the National Research Institute for Earth Science and Disaster Prevention (NIED) for making the KiK-net and K-NET data available. S. Mazzotti kindly provided the strain rate and A. Tanaka the heat flow data, S. Toda and B. Enescu the b values. I thank the editor Peter Shearer, Takuji Yamada, William R. Walter and an anonymous reviewer, as well as N. d'Oreye, S. Parolai, D. Bindi and M. Böse for constructive comments that helped to improve the article.

Appendix

Supplementary material associated with this article can be found in the online version. It contains two sections of Supplementary text, Figures S1 – S9 and Tables S1 – S4.

References

- Abercrombie, R.E., and Rice, J.R., 2005. Can observations of earthquake scaling constrain slip weakening? *Geophys. J. Int.* *162*, 406-424, doi:10.1111/j.1365-246X.2005.02579.x.
- Allmann, B.P., and Shearer, P.M., 2007. Spatial and temporal stress drop variations in small earthquakes near Parkfield, California. *J. Geophys. Res.* *112*, B04305, doi:10.1029/2006JB004395.
- Allmann, B.P., and Shearer, P.M., 2009. Global variations of stress drop for moderate to large earthquakes. *J. Geophys. Res.* *114*, B01310, doi:10.1029/2008JB005821.
- Anderson, J.G., and Hough, S.E., 1984. A model for the shape of the Fourier amplitude spectrum of acceleration at high frequencies. *Bull. Seismol. Soc. Am.* *74*, 1969-1993.
- Baltay, A., Prieto, G., and Beroza, G.C., 2010. Radiated seismic energy from coda measurements and no scaling in apparent stress with seismic moment. *J. Geophys. Res.* *115*, B08314, doi:10.1029/2009JB006736.

- Beroza, G.C., and Ide, S., 2011. Slow Earthquakes and Nonvolcanic Tremor. *Annu. Rev. Earth Planet. Sci.* 39, 271-296, doi:10.1146/annurev-earth-040809-152531.
- Boore, D.M., and Atkinson, G.M., 2007. Boore-Atkinson NGA ground motion relations for the geometric mean horizontal component of peak and spectral ground motion parameters. PEER Report 2007/01.
- Boore, D.M., and Boatwright, J., 1984. Average body-wave radiation coefficients. *Bull. Seismol. Soc. Am.* 74, 1615-1621.
- Brocher, T.M., 2005. Empirical Relations between Elastic Wavespeeds and Density in the Earth's Crust. *Bull. Seismol. Soc. Am.* 95, 2081-2092, doi:10.1785/0120050077.
- Brune, J.N., 1970. Tectonic stress and the spectra of seismic shear waves from earthquakes. *J. Geophys. Res.* 75, 4997-5009.
- Brune, J.N., 1971. Correction. *J. Geophys. Res.* 76, 5002.
- Castro, R.R., Anderson, J.G., and Singh, S.K., 1990. Site response, attenuation and source spectra of S waves along the Guerrero, Mexico, subduction zone. *Bull. Seismol. Soc. Am.* 80, 1481-1503.
- Choy, G.L., and Kirby, S.H., 2004. Apparent stress, fault maturity and seismic hazard for normal-fault earthquakes at subduction zones. *Geophys. J. Int.* 159, 991-1012, doi:10.1111/j.1365-246X.2004.02449.x.
- Cotton, F., Archuleta, R., and Causse, M., 2013. What is Sigma of the Stress Drop? *Seismol. Res. Lett.* 84, 42-48, doi:10.1785/0220120087.
- Das, S., 2007. The Need to Study Speed. *Science* 317, 905-906, doi:10.1126/science.1142143.
- Di Toro, G., Han, R., Hirose, T., De Paola, N., Nielsen, S., Mizoguchi, K., Ferri, F., Cocco, M., and Shimamoto, T., 2011. Fault lubrication during earthquakes. *Nature* 471, 494-498, doi:10.1038/nature09838.
- Gardner, G., Gardner, L., and Gregory, A., 1974. Formation velocity and density - the diagnostic basics for stratigraphic traps. *Geophysics* 39, 770-780, doi:10.1190/1.1440465.
- Goertz-Allmann, B., and Wiemer, S., 2013. Geomechanical modeling of induced seismicity source parameters and implications for seismic hazard assessment. *Geophysics* 78, KS25-KS39, doi: 10.1190/geo2012-0102.1.
- Hanks, T.C., 1982. f_{max} . *Bull. Seismol. Soc. Am.* 72, 1867-1879.

- Hanks, T.C., and Thatcher, W., 1972. A graphical representation of seismic source parameters. *J. Geophys. Res.* 77, 4393-4405.
- Hasegawa, A., Nakajima, J., Uchida, N., Okada, T., Zhao, D., Matsuzawa, T., and Umino, N., 2009. Plate subduction, and generation of earthquakes and magmas in Japan as inferred from seismic observations: An overview. *Gondwana Research* 16, 370-400, doi: 10.1016/j.gr.2009.03.007.
- Hashimoto, C., Noda, A., Sagiya, T., and Matsu'ura, M., 2009. Interplate seismogenic zones along the Kuril-Japan trench inferred from GPS data inversion. *Nature Geosci.* 2, 141-144, doi:10.1038/ngeo421.
- Ide, S., and Beroza, G.C., 2001. Does apparent stress vary with earthquake size? *Geophys. Res. Lett.* 28, 3349-3352.
- Ide, S., Baltay, A., and Beroza, G.C., 2011. Shallow Dynamic Overshoot and Energetic Deep Rupture in the 2011 Mw 9.0 Tohoku-Oki Earthquake. *Science* 332, 1426-1429, doi:10.1126/science.1207020.
- Imanishi, K., Ando, R., and Kuwahara, Y., 2012. Unusual shallow normal-faulting earthquake sequence in compressional northeast Japan activated after the 2011 off the Pacific coast of Tohoku earthquake. *Geophys. Res. Lett.* 39, L09306, doi:10.1029/2012GL051491.
- Kanamori, H., and Heaton, T.H. (2000). Microscopic and macroscopic physics of earthquakes. In *Geocomplexity and the Physics of Earthquakes*, J. Rundle, D. Turcotte, and W. Klein, eds. (American Geophysical Monograph 120).
- Kanamori, H., and Rivera, L., 2004. Static and dynamic scaling relations for earthquakes and their implications for rupture speed and stress drop. *Bull. Seismol. Soc. Am.* 94, 314-319.
- Kato, A., Igarashi, T., Obara, K., Sakai, S., Takeda, T., Saiga, A., Iidaka, T., Iwasaki, T., Hirata, N., Goto, K., Miyamachi, H., Matsushima, T., Kubo, A., Katao, H., Yamanaka, Y., Terakawa, T., Nakamichi, H., Okuda, T., Horikawa, S., Tsumura, N., Umino, N., Okada, T., Kosuga, M., Takahashi, H., and Yamada, T., 2013. Imaging the source regions of normal faulting sequences induced by the 2011 M9.0 Tohoku-Oki earthquake. *Geophys. Res. Lett.* 40, 273-278, doi:10.1002/grl.50104.
- Kurahashi, S., and Irikura, K., 2013. Short-Period Source Model of the 2011 Mw 9.0 Off the Pacific Coast of Tohoku Earthquake. *Bull. Seismol. Soc. Am.* 103, 1373-1393, doi:10.1785/0120120157.

- Madariaga, R., 1976. Dynamics of an expanding circular fault. *Bull. Seismol. Soc. Am.* *66*, 639-666.
- Malagnini, L., Nielsen, S., Mayeda, K., and Boschi, E., 2010. Energy radiation from intermediate to large magnitude earthquakes: implications for dynamic fault weakening. *J. Geophys. Res.* *115*, B06319, doi:10.1029/2009JB006786.
- Mayeda, K., and Malagnini, L., 2010. Source radiation invariant property of local and near-regional shear-wave coda: Application to source scaling for the Mw 5.9 Wells, Nevada sequence. *Geophys. Res. Lett.* *37*, L07306, doi:10.1029/2009GL042148.
- Mayeda, K., Gök, R., Walter, W.R., and Hofstetter, A., 2005. Evidence for non-constant energy/moment scaling from coda-derived source spectra. *Geophys. Res. Lett.* *32*, L10306, doi:10.1029/2005GL022405.
- Mazzotti, S., Henry, P., and Le Pichon, X., 2001. Transient and permanent deformation of central Japan estimated by GPS: 2. Strain partitioning and arc-arc collision. *Earth Planet. Sci. Lett.* *184*, 455-469, doi:10.1016/S0012-821X(00)00336-8.
- Miyake, H., Iwata, T., and Irikura, K., 2003. Source characterization for broadband ground-motion simulation: Kinematic heterogeneous source model and strong motion generation area. *Bull. Seismol. Soc. Am.* *93*, 2531-2545, doi:10.1785/0120020183.
- Nakano S, Yamamoto T, Iwaya T, Itoh J, Takada A, 2001. Quaternary volcanoes of Japan. *Geol. Surv. Japan, AIST*, https://gbank.gsj.jp/volcano-QV/VOL_JP/EN/index.htm (last accessed 05 June 2013).
- Okada, Y., Kasahara, K., Hori, S., Obara, K., Sekiguchi, S., Fujiwara, H., and Yamamoto, A., 2004. Recent progress of seismic observation networks in Japan-Hi-net, F-net, K-NET and KiK-net. *Earth Planets Space* *56*, 15-28.
- Oth, A., Bindi, D., Parolai, S., and Di Giacomo, D., 2010. Earthquake scaling characteristics and the scale-(in)dependence of seismic energy-to-moment ratio: Insights from KiK-net data in Japan. *Geophys. Res. Lett.* *37*, L19304, doi:10.1029/2010GL044572.
- Oth, A., Bindi, D., Parolai, S., and Di Giacomo, D., 2011. Spectral Analysis of K-NET and KiK-net Data in Japan, Part II: On Attenuation Characteristics,

- Source Spectra, and Site Response of Borehole and Surface Stations. *Bull. Seismol. Soc. Am.* *101*, 667-687, doi:10.1785/0120100135.
- Sagiya, T., Miyazaki, S., and Tada, T., 2000. Continuous GPS array and present-day crustal deformation of Japan. *Pure Appl. Geophys.* *157*, 2303-2322.
- Schorlemmer, D., Wiemer, S., and Wyss, M., 2005. Variations in earthquake-size distribution across different stress regimes. *Nature* *437*, 539-542, doi:10.1038/nature04094.
- Seno, T., 1999. Syntheses of the regional stress fields of the Japanese islands. *Island Arc* *8*, 66-79, doi:10.1046/j.1440-1738.1999.00225.x.
- Shearer, P.M., Prieto, G.A., and Hauksson, E., 2006. Comprehensive analysis of earthquake source spectra in southern California. *J. Geophys. Res.* *111*, B06303, doi:10.1029/2005JB003979.
- Singh, S.K., and Ordaz, M., 1994. Seismic energy release in Mexican subduction zone earthquakes. *Bull. Seismol. Soc. Am.* *84*, 1533-1550.
- Suzuki, W., Aoi, S., Sekiguchi, H., and Kunugi, T., 2011. Rupture process of the 2011 Tohoku-Oki mega-thrust earthquake (M9.0) inverted from strong-motion data. *Geophys. Res. Lett.* *38*, L00G16, doi:10.1029/2011GL049136.
- Tanaka, A., 2004. Geothermal gradient and heat flow data in and around Japan (II): Crustal thermal structure and its relationship to seismogenic layer. *Earth Planets Space* *56*, 1195-1199.
- Tanaka, A., Yamano, M., Yano, Y., and Sasada, M., 2004. Geothermal gradient and heat flow data in and around Japan (I): Appraisal of heat flow from geothermal gradient data. *Earth Planets Space* *56*, 1191-1194.
- Toda, S., and Enescu, B., 2011. Rate/state Coulomb stress transfer model for the CSEP Japan seismicity forecast. *Earth Planets Space* *63*, 171-185.
- Toda, S., Stein, R.S., and Lin, J., 2011. Widespread seismicity excitation throughout central Japan following the 2011 M=9.0 Tohoku earthquake and its interpretation by Coulomb stress transfer. *Geophys. Res. Lett.* *38*, L00G03, doi:10.1029/2011GL047834.
- Ueno, H., Hatakeyama, S., Aketagawa, T., Funasaki, J., and Hamada, N., 2002. Improvement of hypocenter determination procedures in the Japan Meteorological Agency. *Quart. J. Seism.* *65*, 123-134 (in Japanese with English abstract).

- Wells, D.L., and Coppersmith, K.J., 1994. New empirical relationships among magnitude, rupture length, rupture width, rupture area, and surface displacement. *Bull. Seismol. Soc. Am.* *84*, 974-1002.
- Yoshida, K., Hasegawa, A., Okada, T., Iinuma, T., Ito, Y., and Asano, Y., 2012. Stress before and after the 2011 great Tohoku-oki earthquake and induced earthquakes in inland areas of eastern Japan. *Geophys. Res. Lett.* *39*, L03302, doi:10.1029/2011GL049729.

Figures

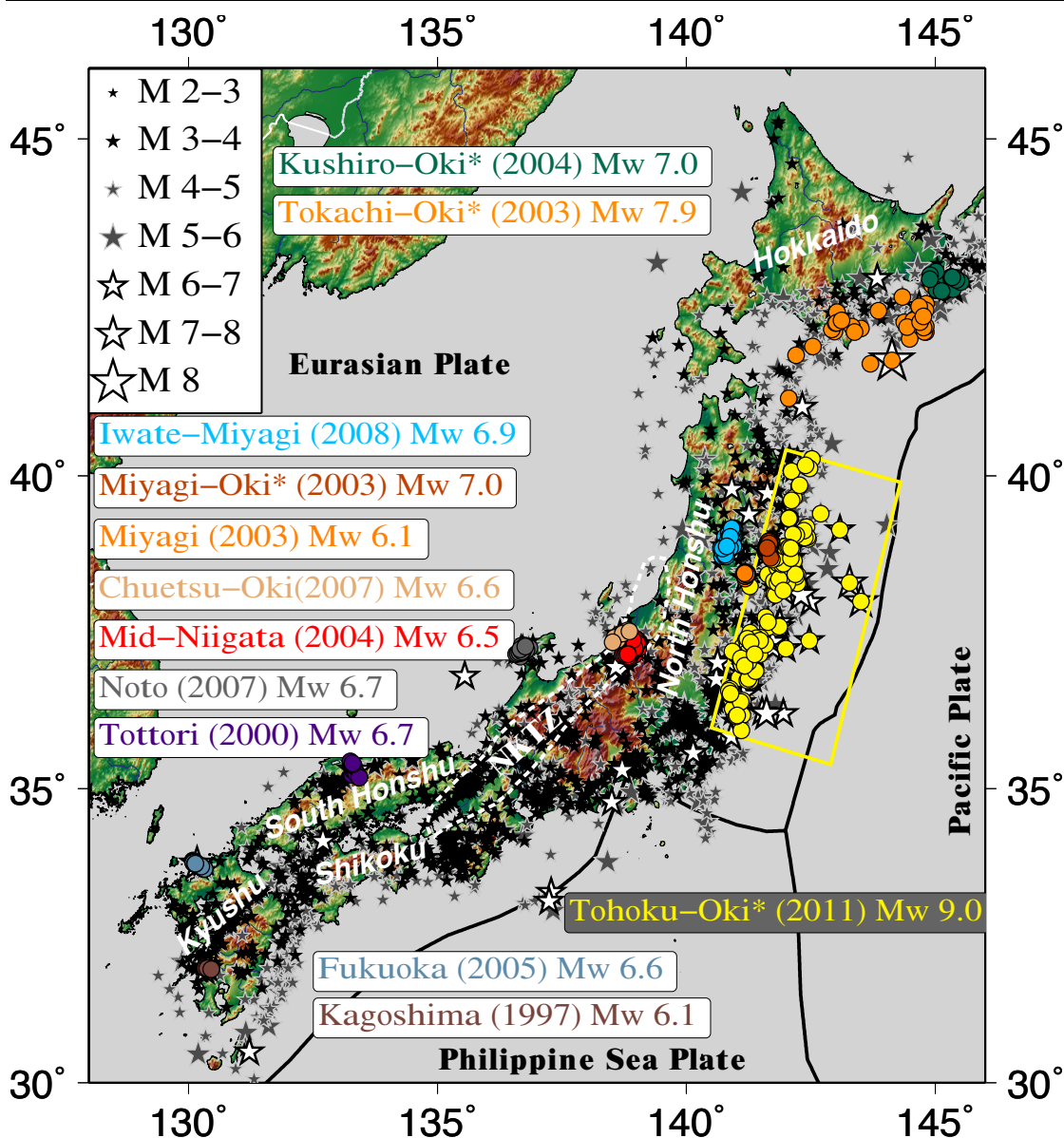


Figure 1: Epicenters of earthquakes used. Extracted individual earthquake sequences are color-coded in relation to mainshock name. Sequences marked with an asterisk are classified as subcrustal. The yellow rectangle indicates the assumed fault model of the Tohoku-Oki mainshock (Suzuki et al., 2011). The Tohoku-Oki mainshock is not included in the spectral inversion (largest event for this sequence is the M_w 7.2 foreshock), but asperity stress drop estimates from empirical Green's functions modeling (Kurahashi and Irikura, 2013) compare well with those expected for subcrustal thrust events (see text).

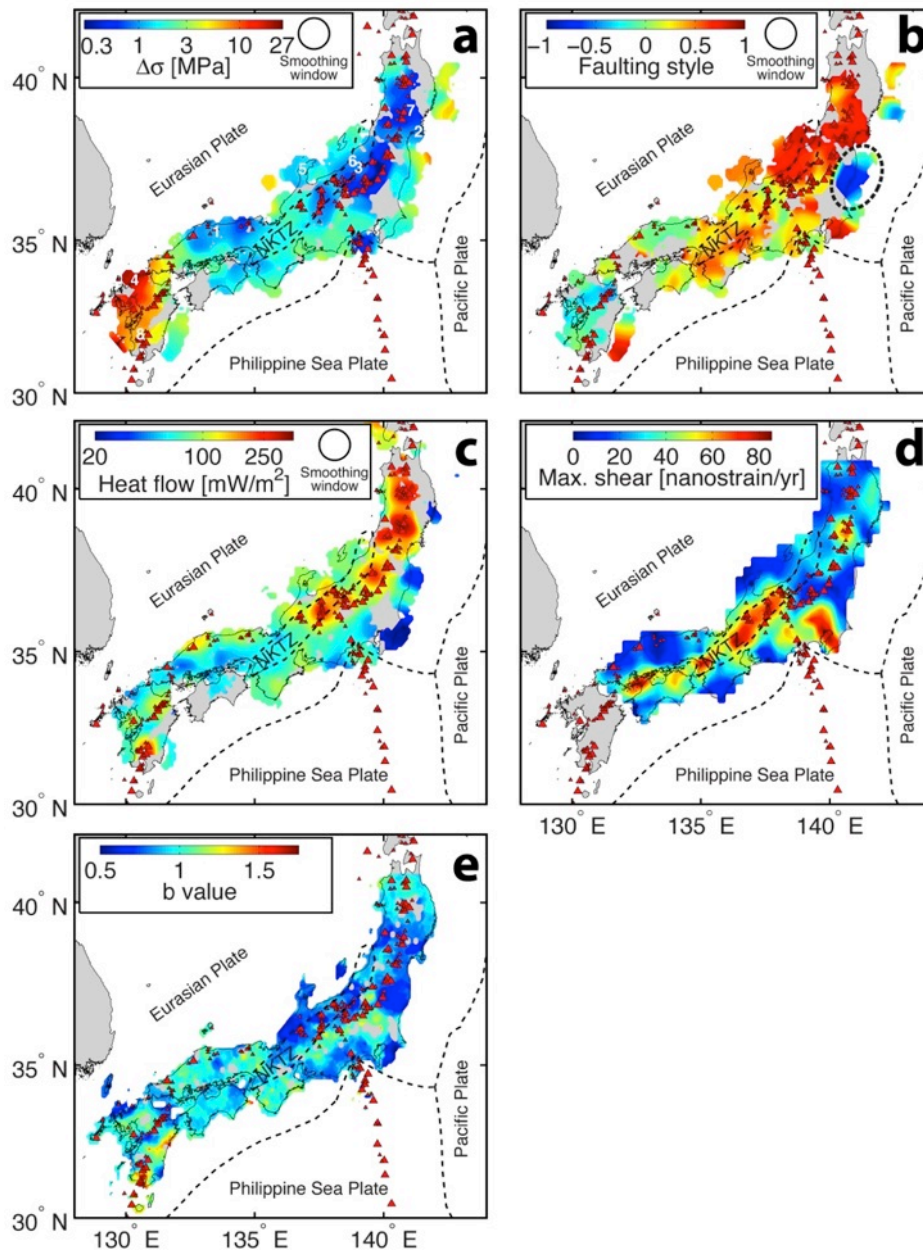


Figure 2: Lateral variation maps in relation to crustal earthquakes. **a**, Crustal earthquake stress drops ($\Delta\sigma$). **b**, Crustal earthquake faulting styles (Shearer et al., 2006) (-1 normal, 0 strike-slip, +1 thrust). **c**, Heat flow (Tanaka et al., 2004). **d**, Residual maximum shear-strain rate in Honshu (Mazzotti et al., 2001). **e**, b values as calculated by Toda and Enescu (2011). NKTZ refers to the Niigata-Kobe Tectonic Zone (see text). Circles in the legends show the extent of the area considered for spatial averaging. White numbers in **a** denote individual sequence locations (see also Fig. 3), and red triangles quaternary volcanoes. Note the normal faulting activity in northeastern Honshu activated in the aftermath of the 2011 Tohoku-Oki earthquake (dashed black ellipse in **b**).

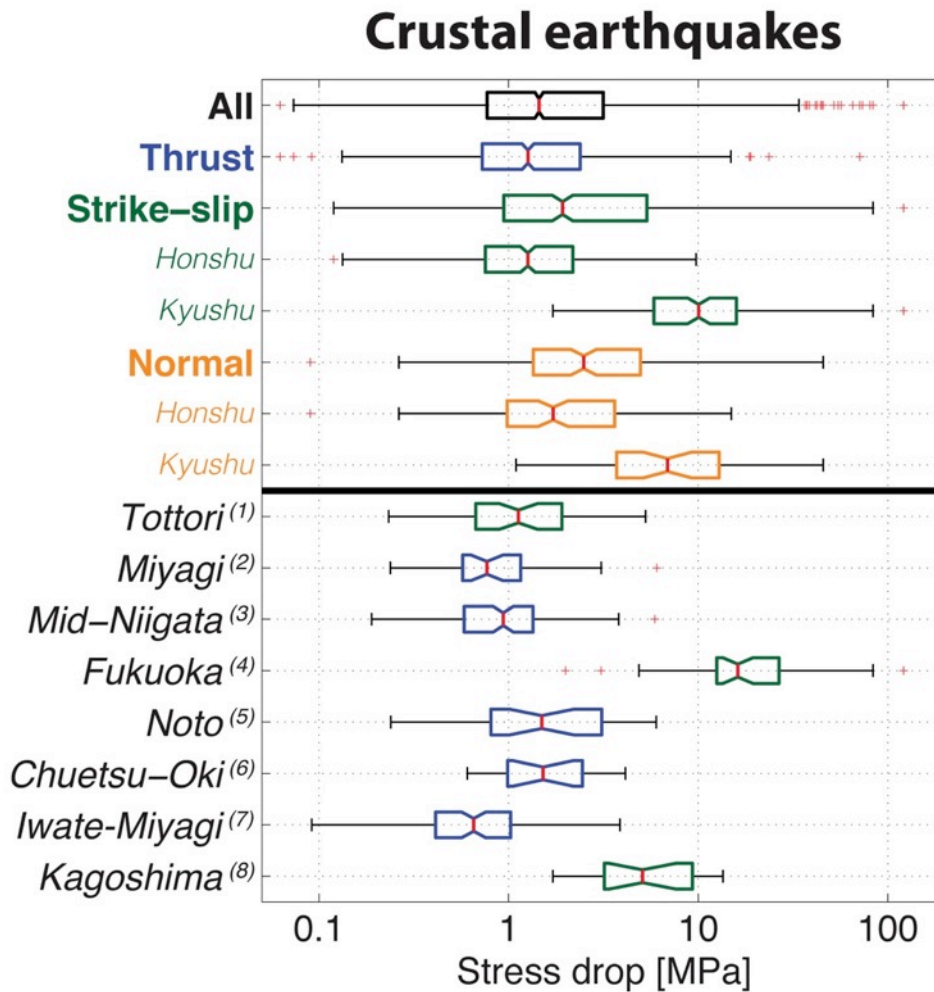


Figure 3: Box and whisker plots of stress drop samples for crustal earthquakes (see also Table S3 in the supplementary material). Red lines indicate median values and boxes show interquartile ranges. Whiskers indicate the data range providing 99.7% coverage of the sample (± 3 standard deviations in case of a Gaussian distribution), remaining outliers are indicated as red crosses. Notches in the boxes provide indications for the significance of different medians, if non-overlapping. The data are ordered in groups according to mechanism and region (top) and individual sequences (bottom, numbered, Fig. 2a).

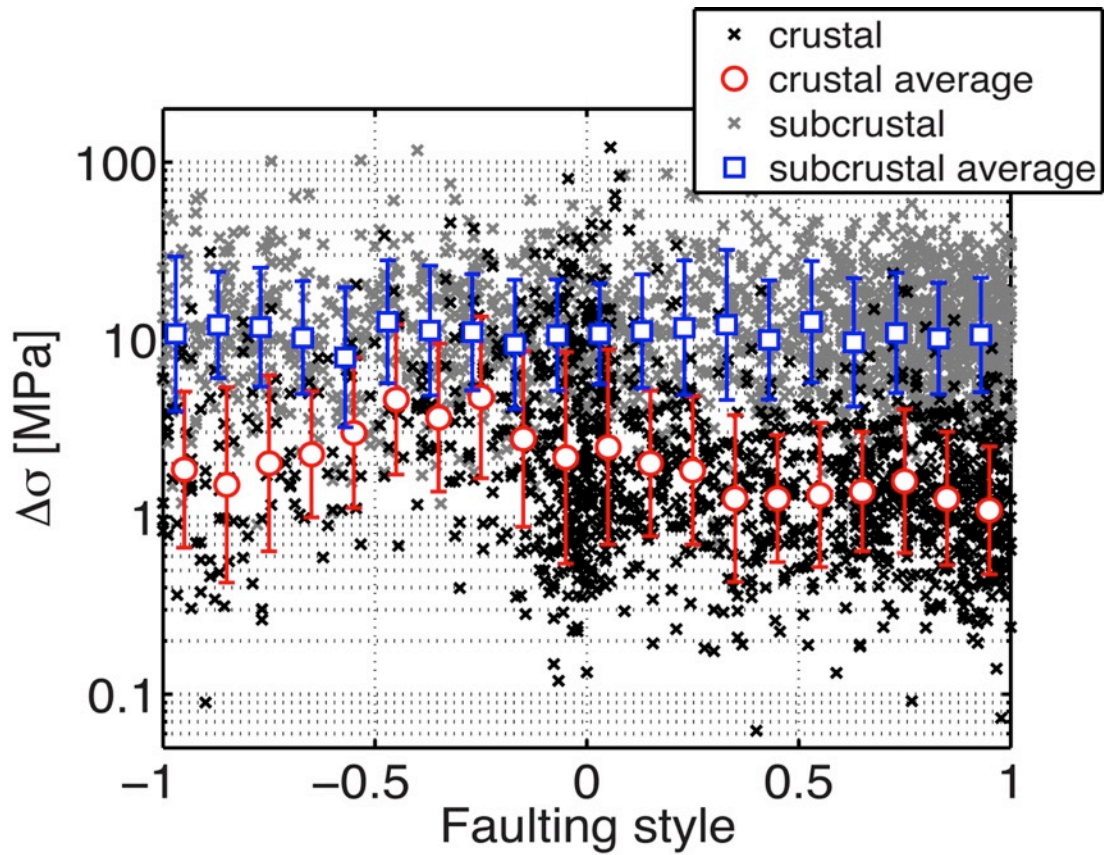


Figure 4: Stress drop dependence on focal mechanism. Note the large variability for crustal strike-slip events (faulting style equal zero) and the slightly elevated stress drops of crustal normal faulting compared to thrust events. Subcrustal earthquakes show no evidence of stress drop mechanism-dependence. Averages were computed in log domain, and the error bars indicate one standard deviation in logarithmic scale.

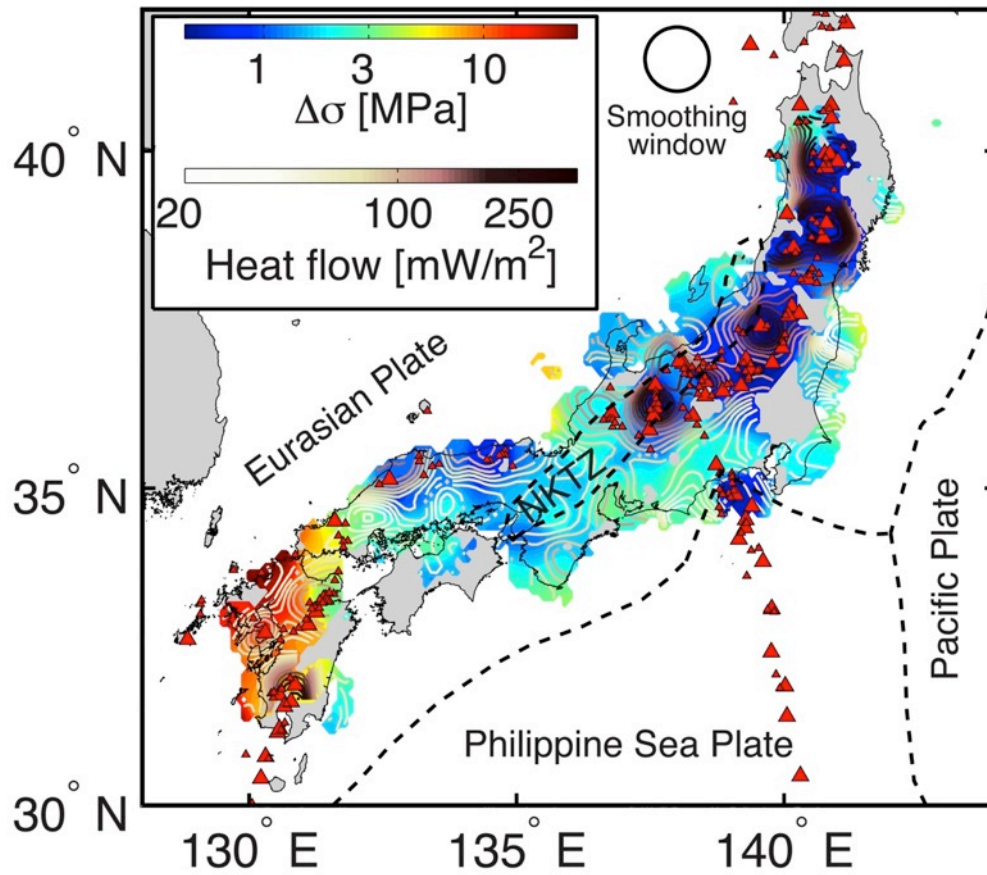


Figure 5: Direct comparison of crustal earthquake lateral stress drop (color-filled areas in background) with heat flow variations (color-coded contour lines in foreground). Note the excellent spatial correlation between the low stress drop and high heat flow regions, in particular in Honshu.

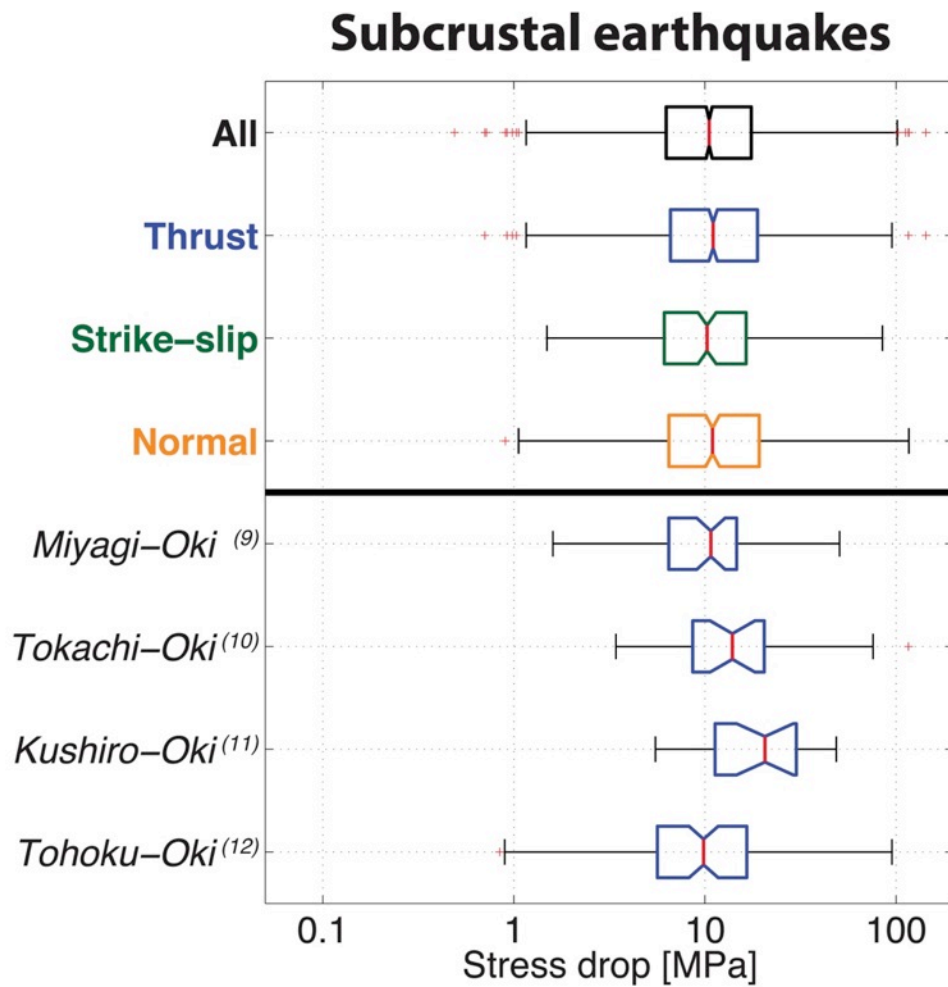


Figure 6: Box and whisker plots of stress drop samples for subcrustal earthquakes (see also Table S4 in the Supplementary material). Same representation as Fig. 3, the locations of the sequences are shown in Fig. 7.

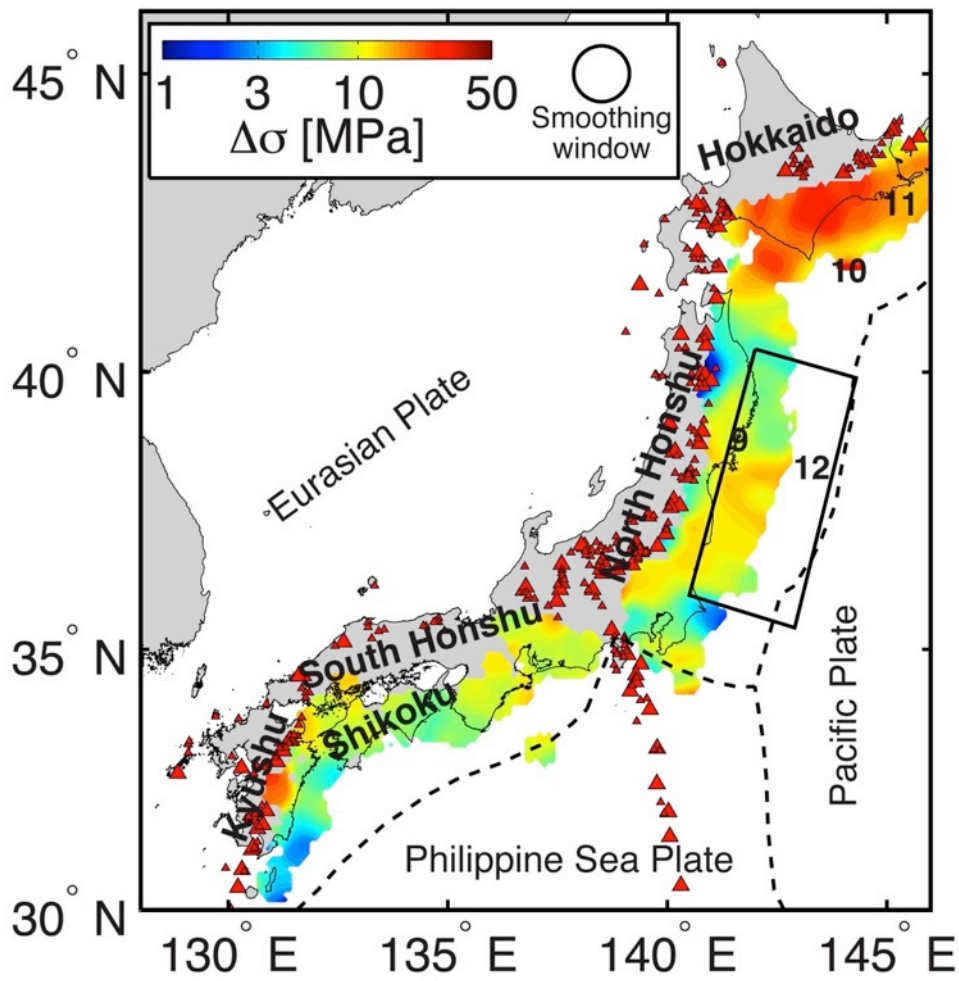


Figure 7: Lateral stress drop variations of subcrustal earthquakes. Numbers denote sequence locations (see also Fig. 6). The assumed fault model of the 2011 Tohoku-Oki earthquake is outlined as black rectangle (Suzuki et al., 2011).

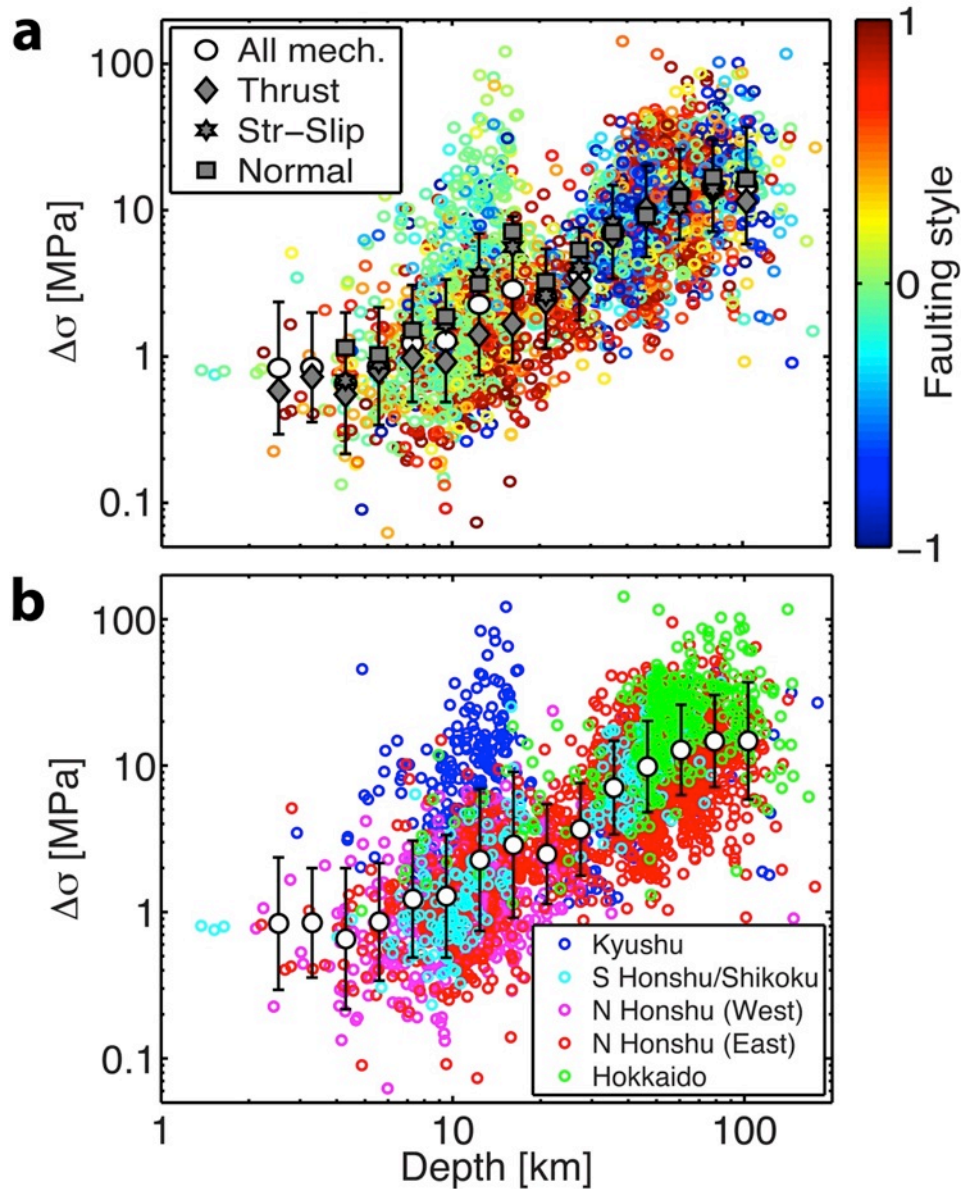


Figure 8: Dependence of stress drop on focal mechanism and depth. **a**, Color-coded with faulting style. **b**, Same as **a**, but color-coded with respect to region. The apparent difference in depth-dependence between strike-slip/normal and thrust events for the crustal depth range is an artifact resulting from the strong lateral variations, as can be seen in **b**. For example, the very high stress drop 2005 Fukuoka sequence strike-slip events in Kyushu generally occurred at slightly larger depths than the 2000 Tottori sequence events, which are associated with low stress drops. This effect is linked to the thickness of the seismogenic layer, which in turn is controlled by the thermal state of the crust. Rather than a real difference in average depth-dependence for different faulting styles, this observation thus reflects the strong lateral variations described in the text.

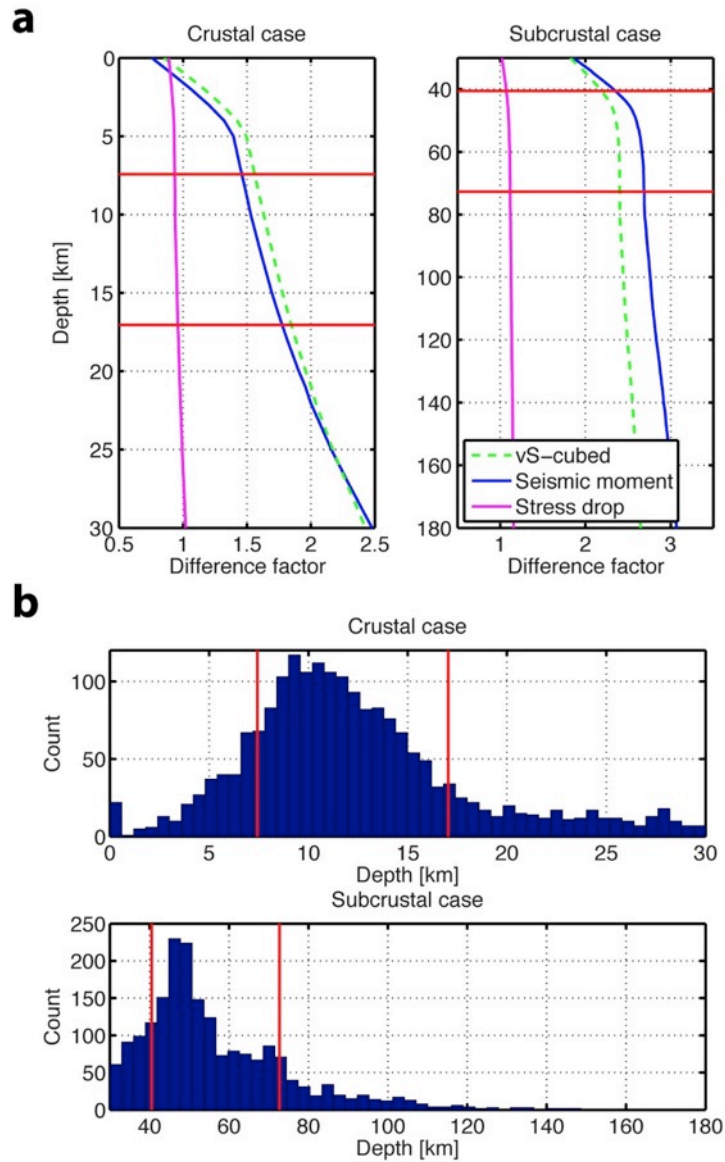


Figure 9: Effect of density and shear-wave velocity depth-dependence on calculated stress drop. **a**, Effect of depth-variable shear-wave velocity v_S and density ρ on seismic moment (blue line), v_S^3 (green dotted line) and stress drop (magenta line), as ratio relative to the estimates of these parameters calculated using constant ρ and v_S . Left: crustal earthquakes, right: subcrustal events. **b**, Histogram plots of the earthquake depth distribution. Top: crustal events, bottom: subcrustal events. Red lines indicate the 16th and 84th percentiles of the distribution, also in a. Due to simultaneous increase in seismic moment and shear-wave velocity cubed, stress drop estimates are nearly unaffected.

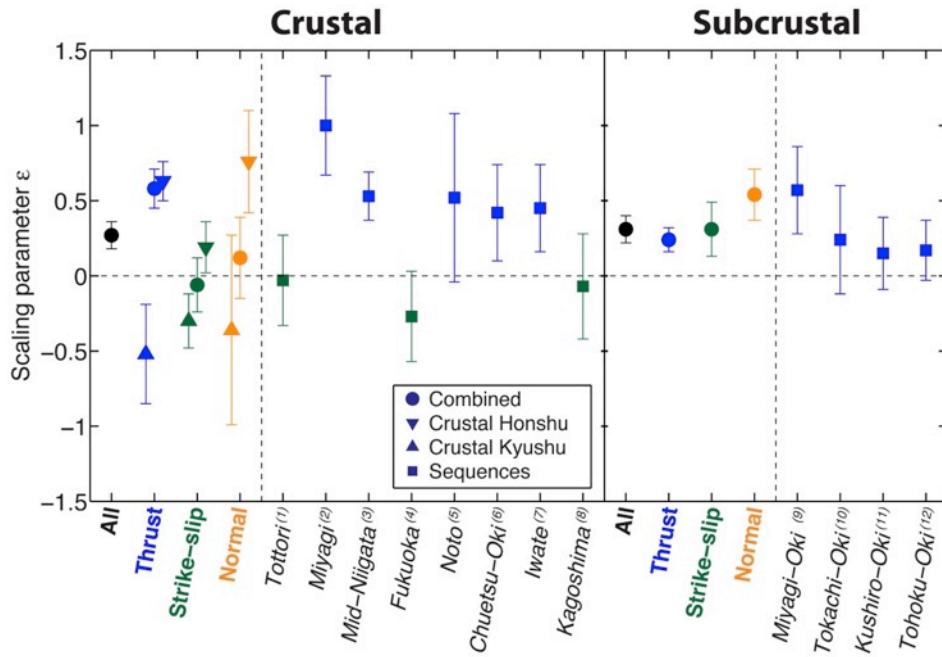


Figure 10: Stress drop scaling with earthquake size (ϵ parameter) and its dependence on faulting mechanism. Recall that $\epsilon=0$ represents self-similarity (i.e., constant stress drop irrespective of magnitude). Squares denote individual earthquake sequences, color-coded according to mechanism. Error bars show the standard deviation estimated through bootstrap resampling. ϵ in Kyushu (triangles) is associated with large uncertainties for thrust and normal faulting (due to few events respectively limited M_W -range, Table S1 in the supplementary material). Note that the Tohoku-Oki sequence scaling is in good agreement with the expectation for subcrustal thrust events.

Tohoku sequence (Mw max 7.2) (2011)

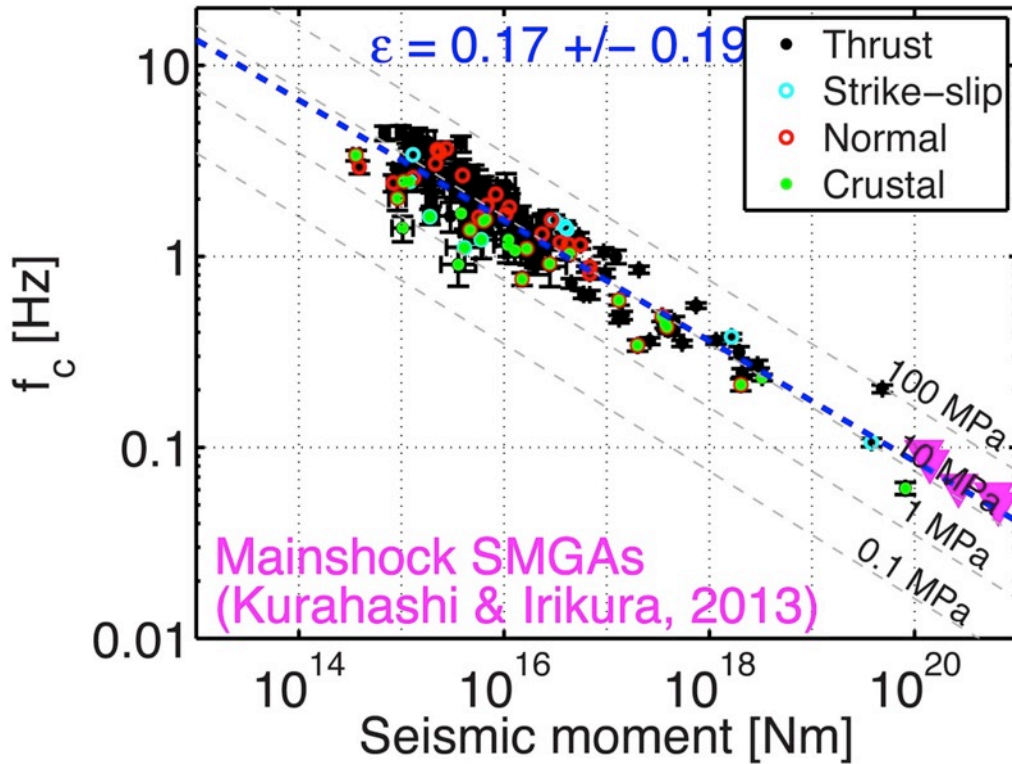


Figure 11: Scaling results in terms of an $f_c - M_0$ plot for the 2011 Tohoku-Oki sequence, with calculated ϵ estimate (see also Table S4 in the supplementary material). Magenta inverse triangles denote the stress drops in the SMGAs derived by empirical Green's functions modeling of the 2011 Tohoku-Oki mainshock (Kurahashi and Irikura, 2013). Note that the SMGA stress drop values of the Tohoku-Oki earthquake were not included when deriving the blue dotted regression line respectively the ϵ estimate.

Supplementary Material

On the characteristics of earthquake stress release variations in Japan

Adrien Oth

European Center for Geodynamics and Seismology (ECGS)
19 rue Josy Welter, L-7256 Walferdange, Grand Duchy of Luxembourg

Contact: adrien.oth@ecgs.lu

TABLE OF CONTENTS:

Section 1

Trade-off between source spectra and attenuation characteristics

While the resulting attenuation functions are as such 1D models, potential regional variations in attenuation characteristics have been taken into account by solving for different crustal attenuation curves in different regions respectively polygons, separating Kyushu, southern Honshu/Shikoku as well as the fore- and backarc regions of northern/central Honshu (see Fig. 1 of Oth et al., 2011, for the definition of these polygons). Thus, even though only 1D, the attenuation model captures potential regional variations, at least to first order.

However, near-source attenuation deviations from the 1D model could nevertheless be a cause of bias in the lateral stress drop variations, so that these would rather represent near-source attenuation variability instead of source variability. While trade-offs between attenuation and source characteristics can never be ruled out with absolute certainty, it is possible to test whether the source- and site-corrected spectral data points of lowest and highest stress drop events in each region follow the 1D attenuation model in the same way as the bulk of the data (moderate stress drop events). Source spectral level is in contrast to attenuation not distance-dependent, so if the source spectral level at a given frequency is strongly “misestimated” due to variations in attenuation structure in the vicinity of the source not captured by the 1D model, the appearance of bias in relation to the distance dependence constrained by the bulk of the data is expected for data points from very high/low stress drop event.

Figure S4 shows examples of this test for crustal earthquakes in all considered regions. Shown are the GIT-derived attenuation functions at a frequency of 10 Hz (chosen as example for the higher frequencies that have the most significant impact on the stress drop estimates – conclusions are identical at other frequencies) in each polygon/region, data points for events with stress drops within the interquartile range as well as data points for the 5% of events with highest and lowest stress drops in each given region.

The spectral amplitudes from the lowest and highest stress drop events in each region follow the 1D attenuation model very well at all distance ranges and with comparable scatter as the bulk of the data, except for a slight bias in southern Honshu and Shikoku, where the highest stress drops seem to be somewhat overestimated in

relation to the attenuation characteristics of the region. However, the events with highest stress drops in southern Honshu/Shikoku are located in the immediate boundary area with the Kyushu region (Fig. 2a in main paper), and furthermore, it appears that these data points would better follow the distance dependence of the Kyushu region rather than the southern Honshu/Shikoku one. It may thus also be the case that the stress drop estimates of these events are not necessarily overestimated, but that the boundary between the Kyushu and southern Honshu/Shikoku regions would have better been slightly differently defined as to include these events into the Kyushu area, which indeed depicts a significantly increased stress drop level. In any case, apart from this small subset that may be debatable, data points from events with very different stress drop levels follow the 1D attenuation model equally well, and this test provides no obvious indications that 2D/3D attenuation deviations from the 1D model would be a significant source of bias regarding the observed lateral stress drop variations.

Section 2

Consistency of seismic moments with NIED CMT solutions

In previous work, we constrained the largest events' moments to the values in the Global Centroid Moment Tensor (GCMT) catalogue (www.globalcmt.org) (Oth et al., 2010). Since GCMT values are not available for earthquakes smaller than about magnitude 5, it is not easily possible to verify the consistency of the determined moments from the smaller events with the GCMT values of the larger ones. Self-consistent moments over the entire range of event sizes are however important to avoid bias in the analysis of stress drop scale-dependence.

In an endeavour to ensure using fully self-consistent moments throughout the entire magnitude range in the dataset, I use the NIED CMT solutions as a benchmark in this work (*The NIED CMT solutions*, <http://www.fnet.bosai.go.jp>). These solutions are available for the vast majority of the smaller earthquakes in the dataset as well as for the large events ($M_{\text{JMA}} \geq 5$), whose moments in the spectral fitting procedure were constrained to the values from the NIED CMT solutions.

This resulted in the choice of slightly different material parameter values as compared to previous work (Oth et al., 2010), since changes in the product ρv_s^3 (see Data and Methods, equation 1) simply reflect in opposite changes in M_0 , with density

and shear wave velocities set to $\rho=2.9 \text{ g/cm}^3$, $v_S=3.0 \text{ km/s}$ and $\rho=2.9 \text{ g/cm}^3$, $v_S=3.3 \text{ km/s}$ for crustal and subcrustal events, respectively, instead of $\rho=2.8 \text{ g/cm}^3$, $v_S=3.5 \text{ km/s}$ and $\rho=3.6 \text{ g/cm}^3$, $v_S=4.2 \text{ km/s}$. Thus, I use adaptations in the material parameters values in order to make the source spectral levels (whose low-frequency amplitude level determines seismic moment) consistent with the expectation from the NIED CMT solutions.

Figure S5 shows that the moments obtained from the spectral fits for earthquakes with $M_{\text{JMA}} < 5$ are consistent with the NIED CMT solutions, and thus also consistent with the moments used as constraints for the larger events ($M_{\text{JMA}} \geq 5$). In particular for the subcrustal case, the revised material parameter values may seem quite low. With these modifications, the overall amplitude level of the source spectra is adjusted so that the moments from the spectral analysis are consistent with the moments of the NIED CMT solutions. The need for this adjustment means, in other words, that the general amplitude level of the inverted source spectra might be a bit higher than one might expect from the NIED CMT solutions. The reason for this slight discrepancy can only be speculated upon. A slightly too strong attenuation correction or a slight remaining amplification effect not fully accounted for by the site response reference condition might play a role. Besides the density and S-wave velocity, other constants need to be set as well (equation 1), and slight modifications in their values would also affect the overall source spectral level.

It should be noted that even if the choice of the constants might well change the absolute values of the stress drop estimates (since S-wave velocity enters in its calculation), stress drop variations within the dataset are not affected by these changes, as long as the same spectral fitting procedure is applied to all events. However, it can play a significant role in terms of scale-dependency studies if, as is the case here, the seismic moments from a subset of the data need to be constrained *a priori*.

References

- Ide, S., and Beroza, G.C., 2001. Does apparent stress vary with earthquake size? *Geophys. Res. Lett.* *28*, 3349-3352.
- Kurahashi, S., and Irikura, K., 2013. Short-Period Source Model of the 2011 Mw 9.0 Off the Pacific Coast of Tohoku Earthquake. *Bull. Seismol. Soc. Am.* *103*, 1373-1393, doi:10.1785/0120120157.
- Oth, A., Bindi, D., Parolai, S., and Di Giacomo, D., 2010. Earthquake scaling characteristics and the scale-(in)dependence of seismic energy-to-moment ratio: Insights from KiK-net data in Japan. *Geophys. Res. Lett.* *37*, L19304, doi:10.1029/2010GL044572.
- Oth, A., Bindi, D., Parolai, S., and Di Giacomo, D., 2011. Spectral Analysis of K-NET and KiK-net Data in Japan, Part II: On Attenuation Characteristics, Source Spectra, and Site Response of Borehole and Surface Stations. *Bull. Seismol. Soc. Am.* *101*, 667-687, doi:10.1785/0120100135.

Supplementary Figures

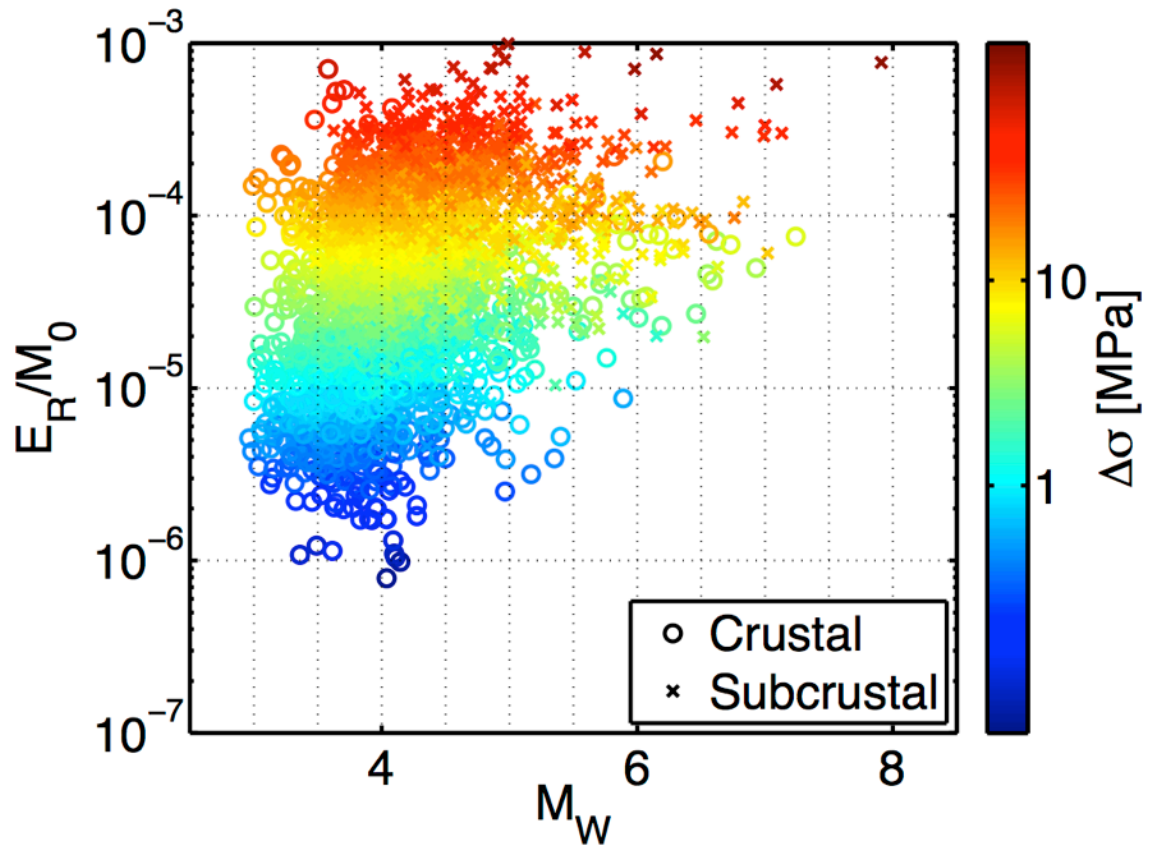


Figure S1

Scaled energy versus seismic moment, color-coded with stress drop estimates.

Scaled energy (seismic energy-to-moment ratio) versus moment magnitude, extrapolated to account for bandwidth limitation (Ide and Beroza, 2001). Data points are color-coded with respect to their stress drop. As already shown in previous work (Oth et al., 2010), scaled energy is highly correlated with stress drop. Overall, there is a large variation in scaled energy values of at least three orders of magnitude and no clear correlation with magnitude.

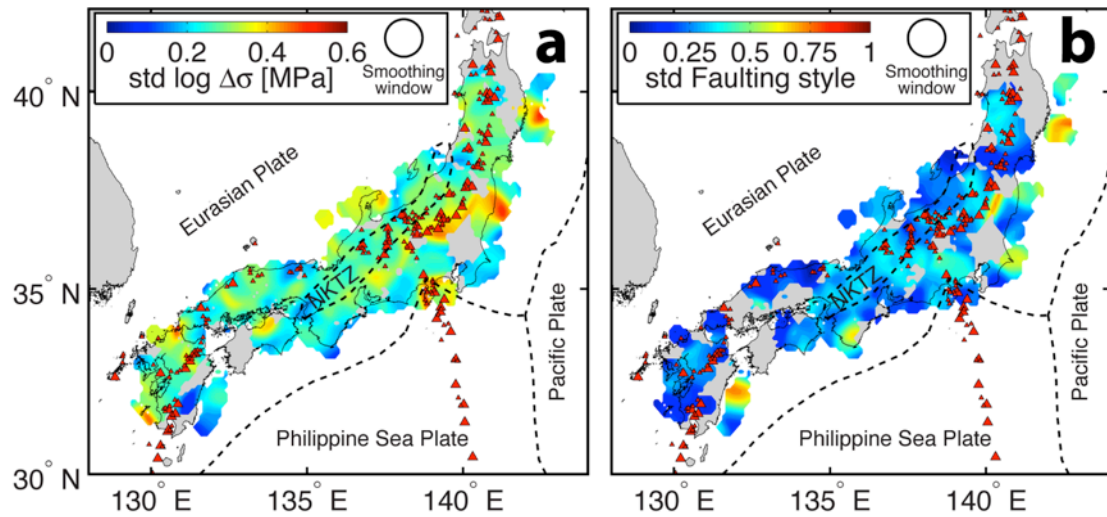


Figure S2

Variability of local samples in lateral variation maps of crustal earthquakes.

a, Standard deviation of the logarithm of stress drop. **b**, Standard deviation of faulting style estimates using the rake-based approach. Note that the local standard deviations are on the same order throughout Japan, without clear spatial pattern, contrasting the clear lateral variations of the estimated local averages.

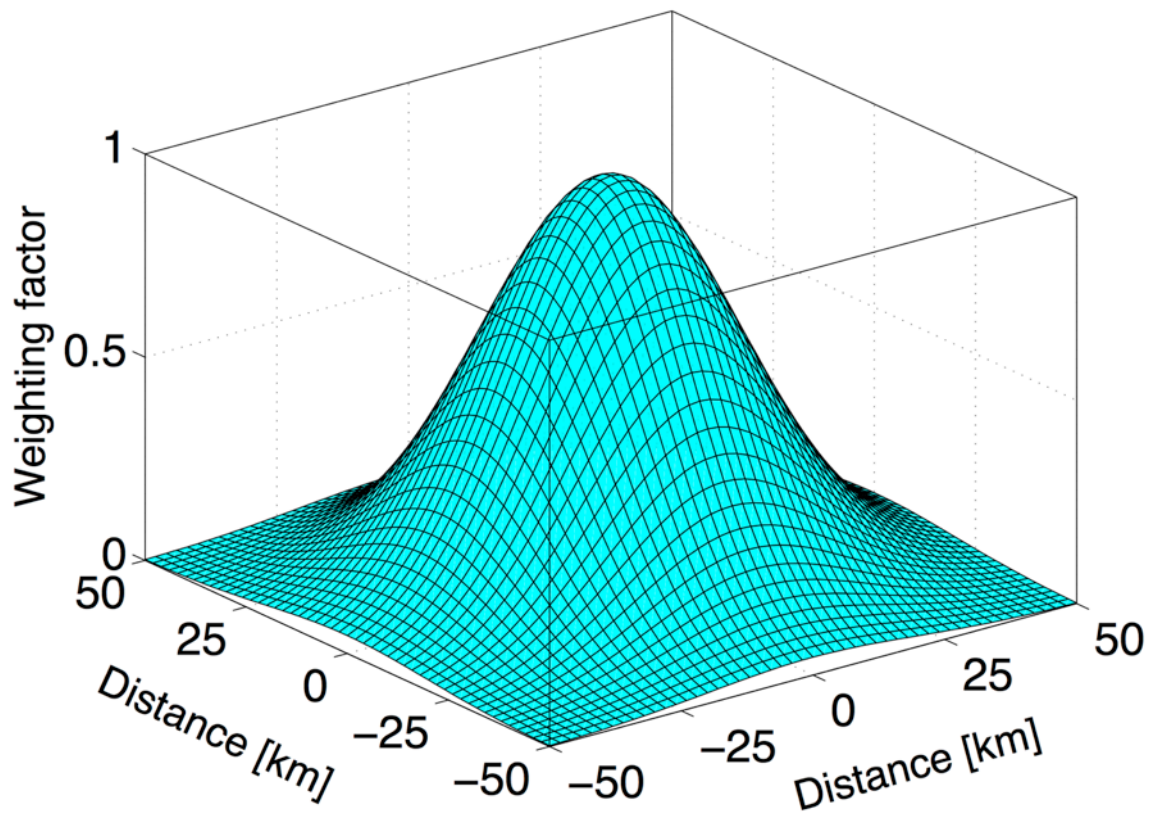


Figure S3

Weighted average operator used for calculating lateral variation maps of stress drop, faulting style and heat flow. The contributions of measurements within a radius of 50 km are weighted relative to their distance from the considered grid point.

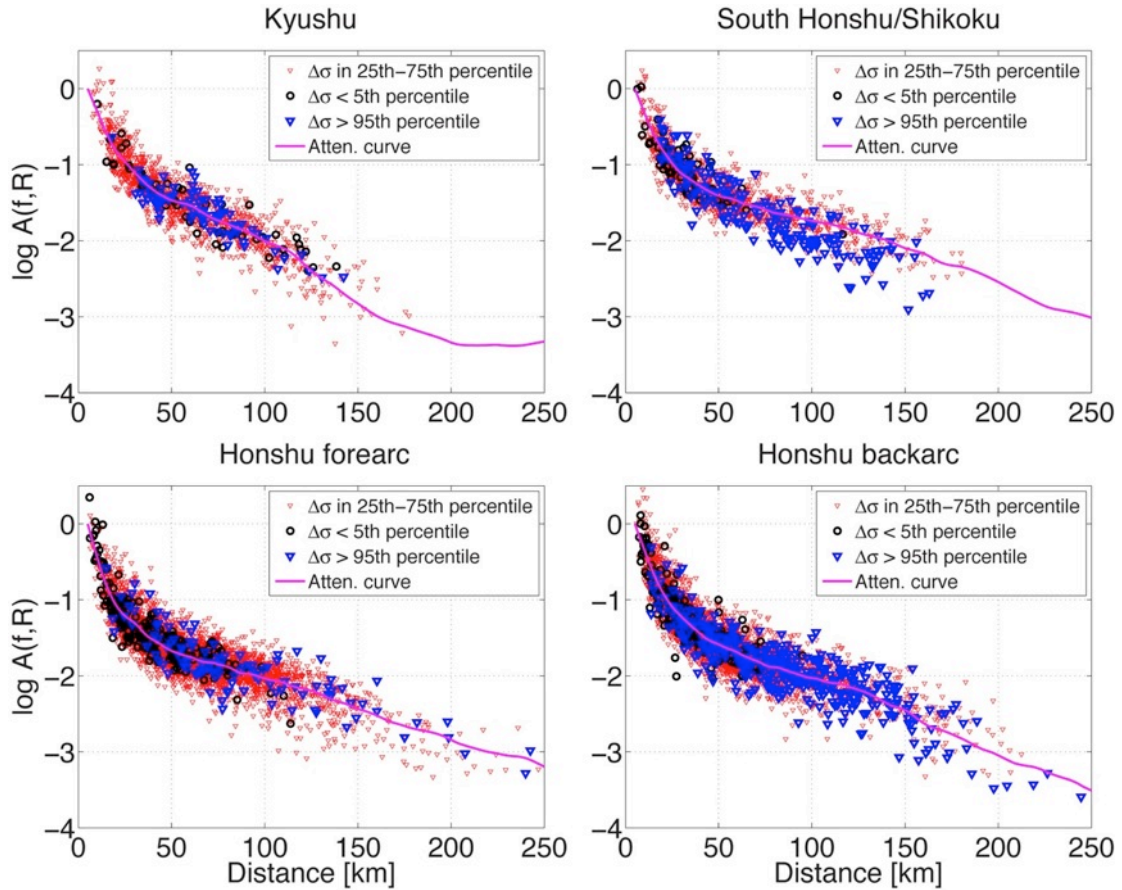
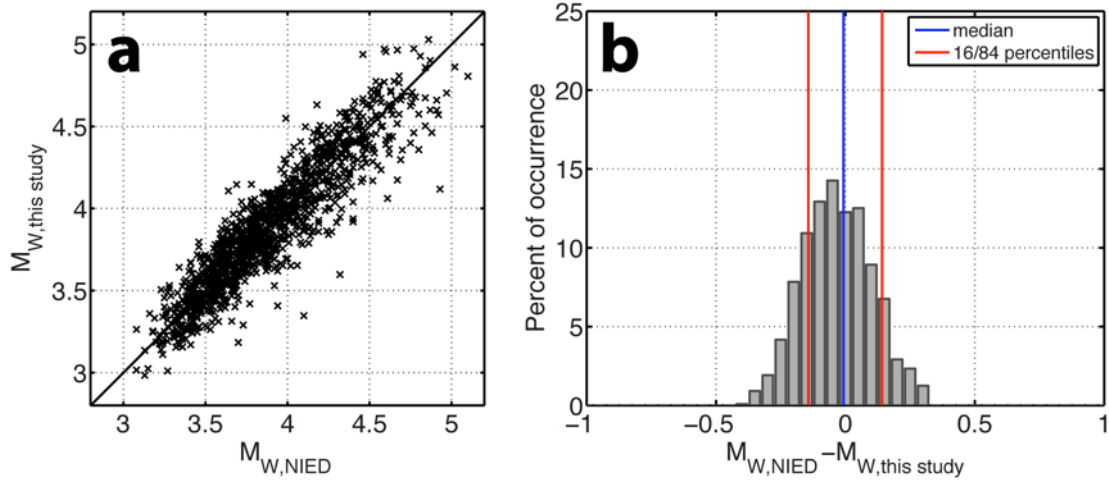


Figure S4

Comparison of source and site-corrected spectral amplitude decay with distance from crustal earthquakes with different stress drop ranges and the inverted attenuation model at frequency 10 Hz in the four considered regions (Oth et al., 2011). Red inverse triangles: data from moderate stress drop events within the interquartile range. Black circles: data from 5% lowest stress drop events. Blue inverse triangles: data from 5% highest stress drop events. Magenta line: 1D attenuation model. Note that except for the highest stress drop events in southern Honshu/Shikoku, spectral amplitudes from events with different stress drop ranges follow the 1D attenuation model equally well.

Crustal events



Subcrustal events

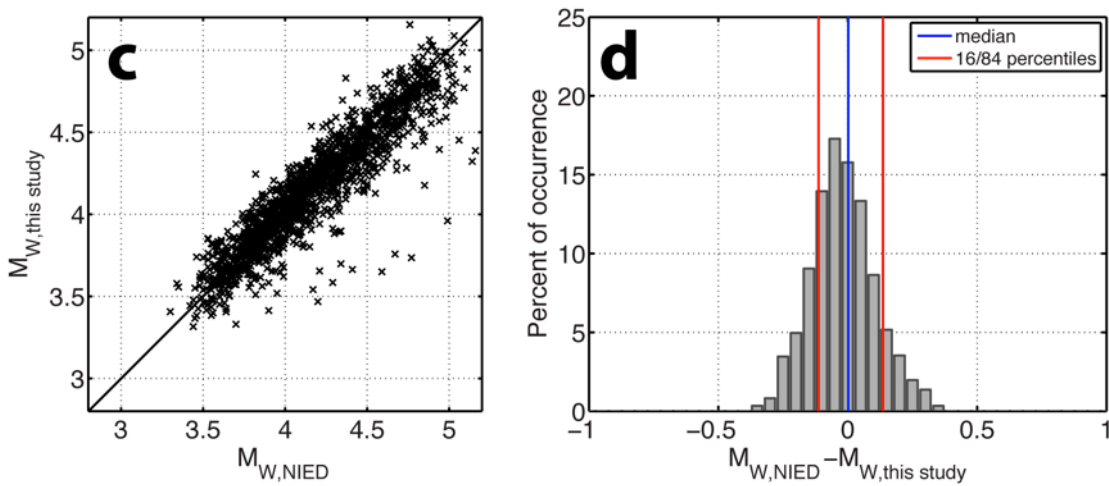


Figure S5

Comparison of moment magnitudes (M_W) as determined in this work for earthquakes with $M_{JMA} < 5$ with the moment magnitudes from the NIED CMT solutions.

a, Direct comparison for crustal earthquakes. **b**, Histogram plot of the magnitude difference. **c**, **d**, Same for subcrustal events. The two M_W estimates are within about 0.1 magnitude units from one another for most events, with unbiased median.

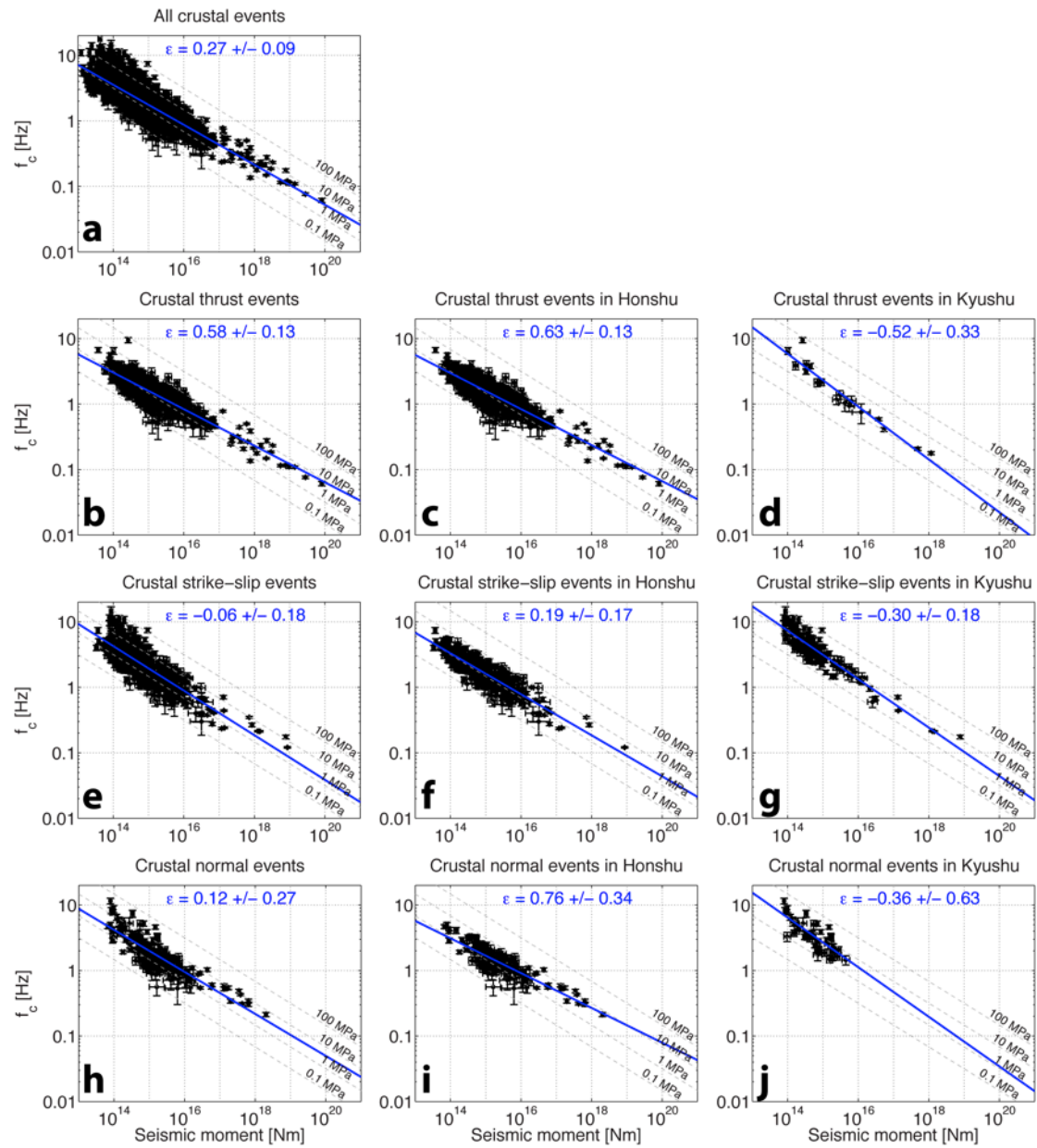


Figure S6

Scaling results in terms of $f_c - M_0$ plots, with calculated ϵ estimate, for crustal earthquakes (see also Table S1). Top row: All crustal events. Second row from top: Thrust events only, with separation of Honshu and Kyushu. Second row from bottom: Same for strike-slip events. Bottom row: Same for normal faulting events. Note the small number of thrust events (d) and the limited magnitude range covered by normal faulting events (j) in Kyushu.

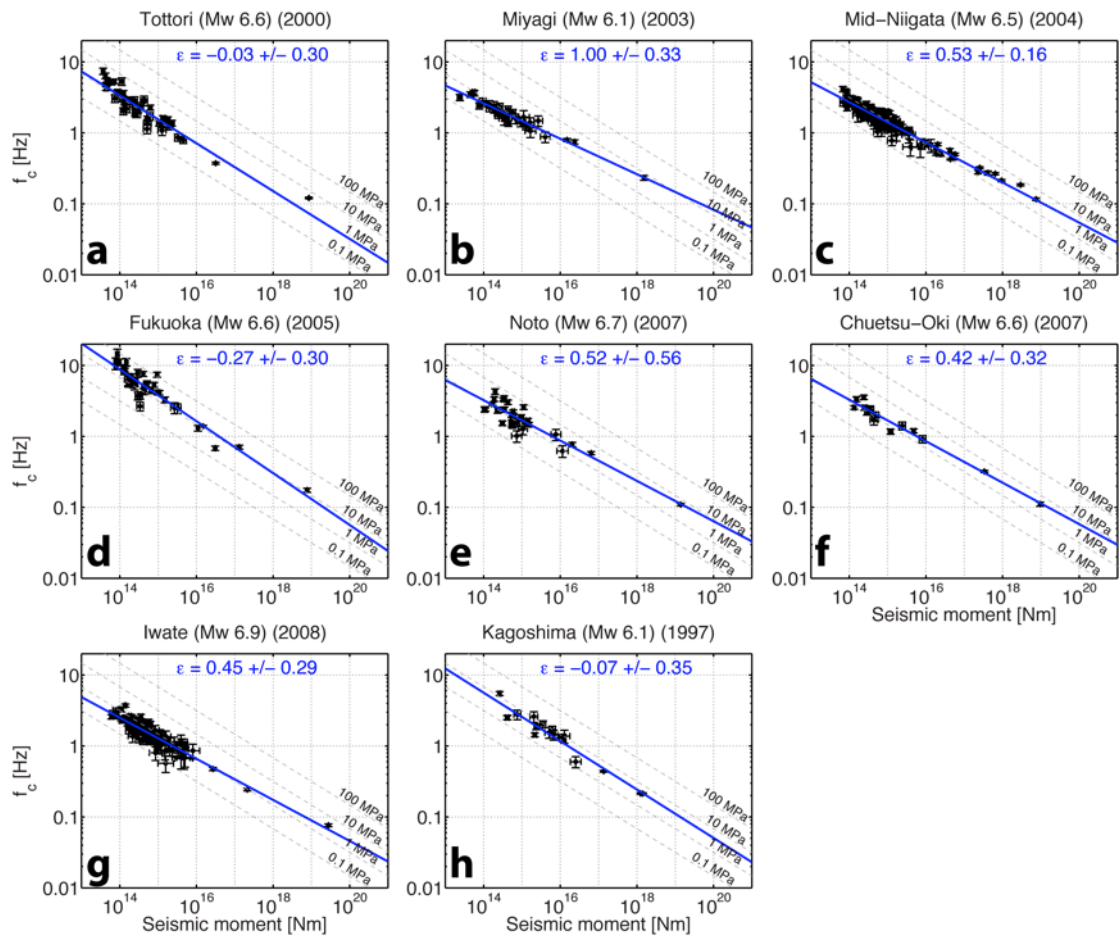


Figure S7

Same as Figure S6, for individual crustal earthquake sequences (see also Table S2).

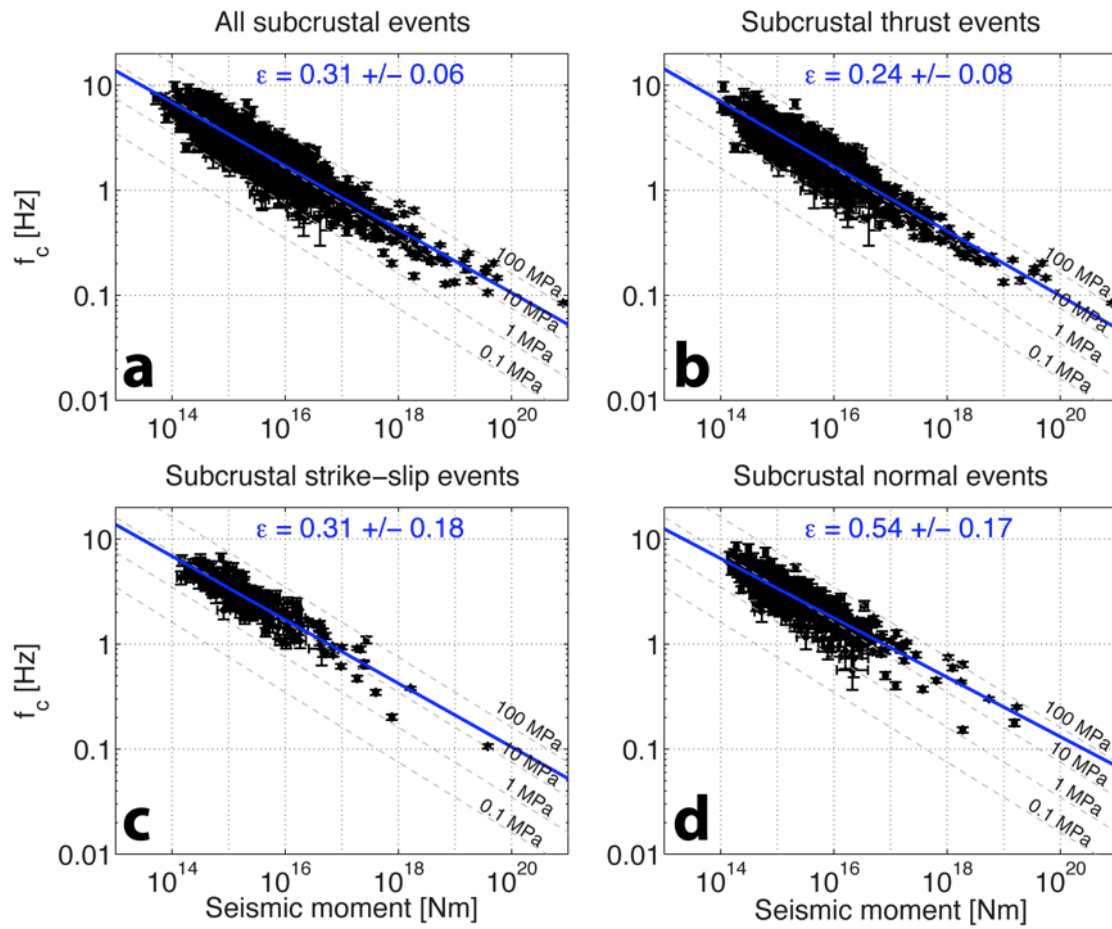


Figure S8

Same as Figure S6 for subcrustal events, separated according to their mechanism (see also Table S1). **a**, All subcrustal events. **b**, subcrustal thrust events. **c**, subcrustal strike-slip events. **d**, subcrustal normal faulting events.

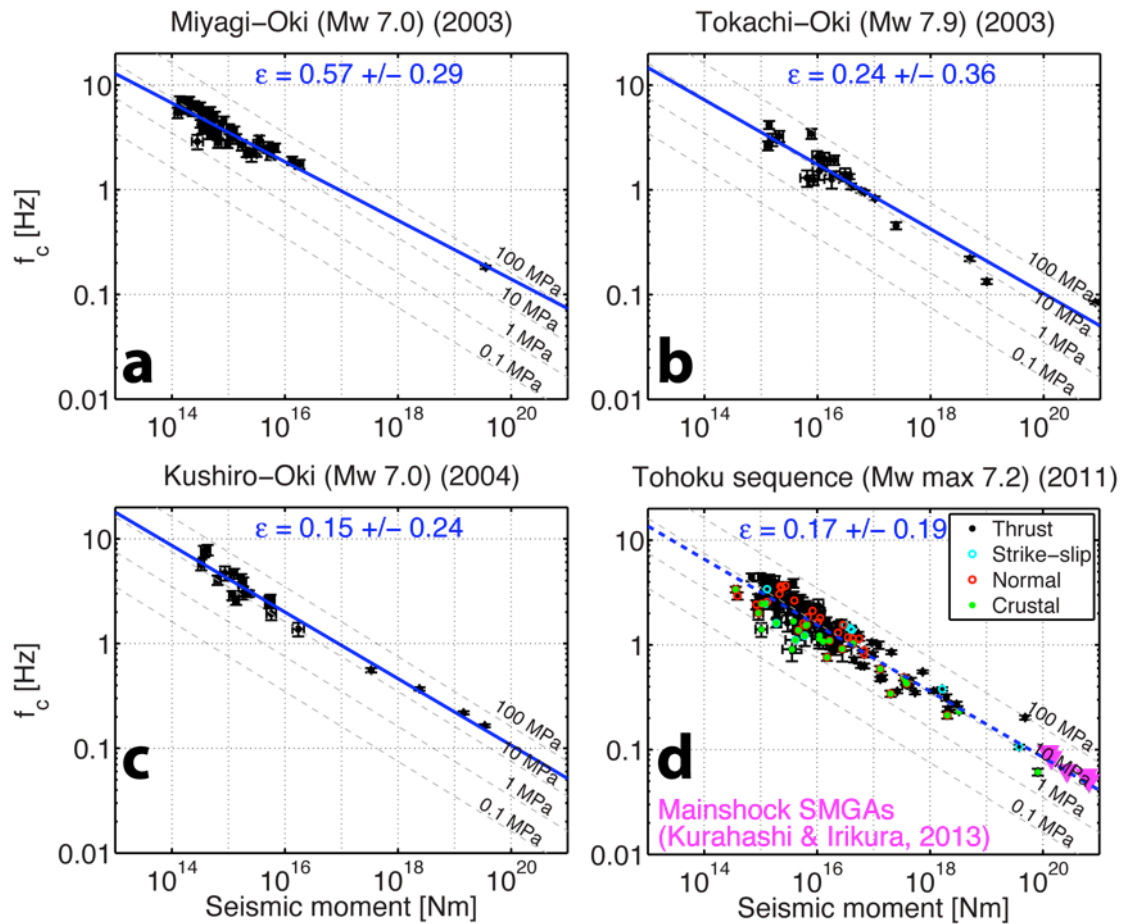


Figure S9

Same as Figure S8, for individual subcrustal sequences (see also Table S2). Note that for the Tohoku sequence in (d), the seismic moment scale (x-axis) is slightly wider. Magenta inverse triangles denote the stress drop in the SMGAs derived by empirical Green's functions modeling of the 2011 Tohoku-Oki mainshock (Kurahashi and Irikura, 2013). Note that in the case of the 2011 Tohoku-Oki earthquake (d), the regression line (blue dotted line) was calculated excluding the SMGA stress drop values.

Supplementary Tables

Table S1.

Dataset characteristics, separated into crustal/subcrustal events, as well as by faulting style and regions in the crustal case. Color-coding visually denotes faulting style, also in Supplementary Tables 2-4. N_{evts} : number of events.

Data subset	N_{evts}	M_W-range
<i>Crustal</i>		
All	1949	2.7 – 7.2
Thrust	693	3.0 – 7.2
Thrust Honshu	675	3.0 – 7.2
Thrust Kyushu	18	3.3 – 6.0
Strike-slip	479	3.0 – 6.6
Strike-slip Honshu	342	3.0 – 6.6
Strike-slip Kyushu	137	3.2 – 6.6
Normal	173	3.2 – 6.2
Normal Honshu	129	3.2 – 6.2
Normal Kyushu	44	3.2 – 4.4
Undefined	604	2.7 – 4.8
<i>Subcrustal</i>		
All	2015	3.1 – 7.9
Thrust	1053	3.3 – 7.9
Strike-slip	201	3.4 – 7.0
Normal	423	3.4 – 6.8
Undefined	338	3.1 – 6.5

Table S2.

List of the twelve earthquake sequences included in this study, color-coded with respect to their faulting style.

Name	N_{evts}	M_w-range	Faulting style	Region
<i>Crustal</i>				
1. Tottori (2000)	49	3.0 – 6.6	strike-slip	Honshu South
2. Miyagi (2003)	32	2.9 – 6.1	thrust	Honshu North
3. Mid-Niigata (2004)	116	3.2 – 6.5	thrust	Honshu North-East
4. Fukuoka (2005)	42	3.2 – 6.6	strike-slip	Kyushu
5. Noto (2007)	29	3.3 – 6.7	thrust	Honshu North-East
6. Chuetsu-Oki (2007)	15	3.4 – 6.6	thrust	Honshu North-East
7. Iwate-Miyagi (2008)	96	3.2 – 6.9	thrust	Honshu North
8. Kagoshima (1997)	17	3.6 – 6.1	strike-slip	Kyushu
<i>Subcrustal</i>				
9. Miyagi-Oki (2003)	56	3.4 – 7.0	thrust	Honshu North
10. Tokachi-Oki (2003)	25	4.0 – 7.9	thrust	Hokkaido
11. Kushiro-Oki (2004)	20	3.6 – 7.0	thrust	Hokkaido
12. Tohoku-Oki (2011)	93	3.9 – 7.2 (9.0*)	thrust	Honshu North-West

*Tohoku-Oki mainshock SMGA stress drop values taken from Kurahashi and Irikura (2013)

Table S3.

Summary of crustal earthquake stress drop distribution and scaling characteristics, tabulated data as shown in Figs. 3 and 10 of main paper. $\Delta\sigma_{25\text{th perc}}$: lower quartile stress drop, $\Delta\sigma_{\text{median}}$: median stress drop, $\Delta\sigma_{75\text{th perc}}$: upper quartile stress drop, ε : scaling parameter, σ_ε : standard deviation of scaling parameter.

Data subset	Stress drop $\Delta\sigma$ [MPa]			Scaling	
	$\Delta\sigma_{25\text{th perc}}$	$\Delta\sigma_{\text{median}}$	$\Delta\sigma_{75\text{th perc}}$	ε	σ_ε
All	0.8	1.4	3.2	0.27	0.09
Thrust	0.7	1.3	2.4	0.58	0.13
Thrust Honshu	0.7	1.2	2.3	0.63	0.13
Thrust Kyushu	1.5	2.5	3.2	-0.52	0.33
Strike-slip	0.9	1.9	5.4	-0.06	0.18
Strike-slip Honshu	0.8	1.3	2.2	0.19	0.17
Strike-slip Kyushu	5.8	10.1	15.9	-0.30	0.18
Normal	1.3	2.5	5.0	0.12	0.27
Normal Honshu	1.0	1.7	3.6	0.76	0.34
Normal Kyushu	3.7	6.9	12.9	-0.36	0.63
Tottori	0.7	1.1	1.9	-0.03	0.30
Miyagi	0.6	0.8	1.2	1.00	0.33
Mid-Niigata	0.6	0.9	1.3	0.53	0.16
Fukuoka	12.5	16.2	26.7	-0.27	0.30
Noto	0.8	1.5	3.1	0.52	0.56
Chuetsu-Oki	1.0	1.5	2.5	0.42	0.32
Iwate	0.4	0.7	1.0	0.45	0.29
Kagoshima	3.2	5.1	9.3	-0.07	0.35

Table S4.

Summary of subcrustal earthquake stress drop distribution and scaling characteristics, tabulated data as shown in Figs. 6 and 10 of main paper. $\Delta\sigma_{25\text{th perc}}$: lower quartile stress drop, $\Delta\sigma_{\text{median}}$: median stress drop, $\Delta\sigma_{75\text{th perc}}$: upper quartile stress drop, ε : scaling parameter, σ_ε : standard deviation of scaling parameter.

Data subset	Stress drop $\Delta\sigma$ [MPa]			Scaling	
	$\Delta\sigma_{25\text{th perc}}$	$\Delta\sigma_{\text{median}}$	$\Delta\sigma_{75\text{th perc}}$	ε	σ_ε
All	6.3	10.5	17.5	0.31	0.06
Thrust	6.6	11.0	18.8	0.24	0.08
Strike-slip	6.1	10.3	16.4	0.31	0.18
Normal	6.5	11.0	19.2	0.54	0.17
Miyagi-Oki	6.5	10.7	14.6	0.57	0.29
Tokachi-Oki	8.6	13.9	20.4	0.24	0.36
Kushiro-Oki	11.3	20.6	30.0	0.15	0.24
Tohoku-Oki	5.6	9.8	16.5	0.17	0.19